

FAINT MEMBERS OF DISTANT GALAXY GROUPS

FAINT MEMBERS OF DISTANT GALAXY GROUPS

By

ROBERT D. E. HENDERSON, BSc

A Thesis

Submitted to the School of Graduate Studies

in Partial Fulfilment of the Requirements

for the Degree

Master of Science

McMaster University

©Copyright by Robert Henderson, July 2010

MASTER OF SCIENCE (2010)
(Department of Physics and Astronomy)

McMaster University
Hamilton, Ontario

TITLE: Faint Members of Distant Galaxy Groups

AUTHOR: Robert Henderson, BSc

SUPERVISOR: Dr. Laura Parker, PhD

NUMBER OF PAGES: xv, 81

Abstract

In this thesis, we present an analysis of ten galaxy groups at $z \sim 0.4$ using spectroscopic data from the FORS2 instrument on the VLT. This study targets group member galaxies at magnitudes fainter than any previous study at this redshift. Our group sample comes from the Group Environment and Evolution Collaboration, which was originally based upon the second Canadian Network for Observational Cosmology redshift survey. Fifty-two new group members are identified, mostly within the apparent magnitude range of $21.25 < r < 23.25$; this accounts for an approximate increase of 25 per cent in the membership of these groups. We combine these new data with previously-obtained follow-up spectroscopy and an extensive set of multiwavelength data to compute composite group galaxy luminosity functions and red fractions. Results from the whole sample are compared with subsamples defined by cuts in group velocity dispersion, radius, and absolute magnitude. Our results indicate that the group environment contains proportionately more bright galaxies than the field (but similar numbers of faint galaxies) and displays little evidence for strong evolution of the luminosity function upon a comparison with lower-redshift samples. In terms of colour, group galaxies are consistently redder than the field. However, there is a strong trend of decreasing red fraction toward fainter magnitudes, in which the group and field environment become statistically similar near the magnitude limit of our sample. The faintest galaxies in our sample are thus predominantly blue, and located in regions outside the virial radius as defined by R_{200} . Overall, our sample's colours follow a

general trend of increasing group red fraction with decreasing redshift, as we show in a comparison with the literature.

Acknowledgements

Allow me to preface this statement by saying that the work in this master's thesis is the culmination of a multitude of experiences, discussions, courses, interactions and opportunities that would not, in any way, have been possible without the gracious assistance and presence of others. The following is an attempt to convey my gratitude for the growth I have managed to build over the past two years.

Quite deserving of acknowledgement are those jovial characters that are (and were) my fellow graduate students, whether they had to endure my presence intra-office or listening to strong opinions at the lunch table. Particularly, I do thank: the strong-willed, detail-oriented Alana Krider and her partner-in-crime, Sarah Nickerson, for many stimulating discussions and their persistent friendship despite Union issues; Benjamin Jackel and Jerod Wagman for their collegial swordsmanship; Blair Cardigan-Smith, Robert Cockcroft, Dennis Duffin, Evert Glebbeek, Jennifer Golding, David Kirsh, Mikhail Klassen, Patrick Rogers, Maximilien Schirm, Sijing Shen, Brendan Sinnott, Rachel Ward, Jeremy Webb, Kristin Anne Woodley and Rory Woods for so many interesting stories of TA-ing, the Planetarium, life, the Universe and everything; Tara Parkin, who was (and is) always willing to chat; and, finally, to all of my astronomical (and non-astronomical) friends and those who are too many to mention.

Owed a great deal of thanks are the fantastic systems administration team, who have not only always been able to solve my computer issues, but in far less time than can ever be reasonably expected by even the most optimistic of people. Specifically, I wish to acknowledge the generous help from Hua Wu, who went above and beyond his job description to assist me with my laptop, and Doug Welch, for solving

my tricky astronomy software problems. The (now former) associate chair, Kari Dalnoki-Veress, was a dedicated and enthusiastic engine of the graduate program when I joined McMaster, and I would like to thank him for his assistance during the course of my degree. Also, I must thank the office staff: Cheryl Johnson, Tina Stewart, Rosemary McNeice, Mara Esposto and Liz Penney for their kind help with administrative matters.

On the academic side of things, there were many people from whom I received much-welcomed assistance in my research. As if supervising me for a summer research project and senior undergraduate thesis wasn't enough, Michael Balogh has kindly continued to be of immense assistance, and this work has benefitted a great deal from his insight and suggestions. Equally helpful have been David Wilman and Jennifer Connelly, who provided me with the software for adapting my FORS2 data to our redshift determination code (which was so kindly provided by Renbin Yan and David Gilbank). David Wilman also assisted heavily with discussions and suggestions for my analysis. Annie Hou and I also had many interesting and informative discussions on our respective research projects. In addition, I would like to thank our entire collaboration, the GEEC, and the members of my supervisory committee, Christine Wilson and Ethan Vishniac, for many helpful comments and suggestions on this work. And, of all the academic help I have had, I thank especially my supervisor, Laura Parker, for her support, insight and patience.

There is a faculty member at McMaster that is uniquely and highly deserving of my gratitude and respect: Reza Nejat. He taught me a great deal about teaching, philosophy and life, and I am grateful to know him. Not too far away, at Waterloo, is Gretchen Harris, another professor who has provided me a great deal of intellectual wisdom. She, thankfully, has always been happy to chat for nearly my entire post-secondary career.

Of course, my family, and especially my parents, deserve a lot more thanks than I can give for all they have done to support me through my studies.

Finally, and most warmly, I thank the love of my life, Carolyn Augusta. She has a knack for making even the most grim of times melt away to reveal all that is good.

Dedicated to Carolyn Augusta and our families.

Table of Contents

| | |
|---|-----------|
| Abstract | iii |
| Acknowledgements | v |
| List of Figures | xiii |
| List of Tables | xv |
| Chapter 1 Introduction | 1 |
| 1.1 Galaxies | 1 |
| 1.2 Galactic Environments | 3 |
| 1.3 Observations of Environments and Interactions | 4 |
| 1.4 Galaxy Groups | 6 |
| 1.5 Galactic Evolution Over Time | 7 |
| 1.6 Current Issues and Questions | 9 |
| 1.7 Thesis Objectives | 11 |
| Chapter 2 The Data | 13 |
| 2.1 The GEEC Galaxies | 13 |
| 2.2 Photometry | 17 |
| 2.2.1 Other Sources | 18 |
| 2.3 Previous Follow-up Spectroscopy | 19 |
| 2.4 Observations and Data Reduction | 19 |

| | | |
|------------------|--|-----------|
| 2.4.1 | Redshift Determination | 24 |
| 2.5 | Summary of the Data | 29 |
| Chapter 3 | Analysis and Results | 31 |
| 3.1 | Galaxy Group Membership | 31 |
| 3.2 | Completeness Corrections | 33 |
| 3.3 | Luminosities and Colours | 38 |
| 3.3.1 | Photometric Limits | 38 |
| 3.3.2 | K-corrections | 40 |
| 3.3.3 | Colours | 44 |
| 3.4 | Luminosity Functions | 48 |
| 3.4.1 | A Comparison Between Red and Blue Galaxies | 51 |
| 3.4.2 | Trends in Group Mass | 53 |
| 3.5 | Red Fractions | 56 |
| Chapter 4 | Discussion and Conclusions | 59 |
| 4.1 | Radial Trends | 59 |
| 4.2 | Dynamical Effects of the Faint Galaxies | 60 |
| 4.3 | Evolution | 62 |
| 4.3.1 | Low-redshift Luminosity Functions | 64 |
| 4.3.2 | Evolution in Group Galaxy Colours | 65 |

| | | |
|------------------|------------------------------|-----------|
| Chapter 5 | Conclusions | 69 |
| 5.1 | Future Work | 70 |
| 5.2 | Concluding Remarks | 71 |

List of Figures

| | | |
|------|---|----|
| 2.1 | CNOC2 14hr Field | 14 |
| 2.2 | CNOC2 21hr Field | 15 |
| 2.3 | Distribution of Group Velocity Dispersions | 21 |
| 2.4 | The ZSPEC Program Interface | 26 |
| 2.5 | Examples of Redshift Quality Flags and Spectra | 27 |
| 2.6 | Redshift Success Rate | 28 |
| 2.7 | Velocity Differences in a Comparison Sample of Previous Redshifts | 30 |
| 3.1 | Radial Velocity Differences of Galaxies and Our Groups | 34 |
| 3.2 | Selection Functions | 37 |
| 3.3 | Colour versus Apparent r Magnitude | 41 |
| 3.4 | Photometric Number Counts for Various Filters | 42 |
| 3.5 | K-correction Colours Before and After | 45 |
| 3.6 | Colour-Magnitude Diagram with Red Sequence Fit | 46 |
| 3.7 | Distribution of $^{0.4}(g - r)$ Colours | 47 |
| 3.8 | Luminosity Functions for the Group and Field Samples | 52 |
| 3.9 | Composite Group Luminosity Function Split by Colour | 54 |
| 3.10 | Composite Group Luminosity Functions for the Low- and High- σ Samples | 55 |

| | |
|--|----|
| 3.11 Red Fraction as a Function of Mangitude for the Group and Field Samples | 58 |
| 4.1 Composite Group Luminosity Functions with Radial Cuts | 61 |
| 4.2 Our Low- σ Groups Compared with the GEMS Low- z , Low X-ray Groups | 66 |
| 4.3 Our High- σ Groups Compared with the GEMS Low- z , High X-ray Groups | 67 |

List of Tables

| | | |
|-----|---|----|
| 2.1 | Basic Data on Our GEEC Group Sample | 22 |
| 3.1 | Red Fractions | 57 |
| 4.1 | Dynamical Classifications | 63 |

Chapter 1

Introduction

1.1 Galaxies

Most of our knowledge about the Universe is drawn from observations of galaxies, be it our own or those at the greatest conceivable distances. Observing these collections of stars, gas, dust and elusive ‘dark’ matter can tell us many things about their history, evolution and environment. For example, by simply looking at a galaxy’s colour we can tell something about its age (e.g. Strateva et al., 2001).

Another very important measurement we can make, and without knowledge of distance, is the shape of galaxies. This can be a qualitative visual classification into one of several types on the Hubble sequence (Hubble, 1926) or quantitatively by fitting the radial distribution of surface brightness (e.g. Simard et al., 2002; Driver et al., 2005; McGee et al., 2008). In both methods, it is well-established that there is a bimodal population of galaxy morphology: the *early types* (often *elliptical* in shape) are characterised by a large central bulge in which the old, red stars are mostly on randomised orbits (but see

Krajnović et al., 2008); the *late types* (often *spiral*-shaped) are disk-dominated with younger, bluer stellar populations that coherently rotate about the centre of the galaxy (e.g. Terndrup, 1993; Proctor et al., 2000; Peletier & Balcells, 1996). There is also a class of morphology, referred to as the lenticular galaxies (or *S0s*) which feature a dominant bulge and a non-star-forming disk. These turn out to be an important class of galaxies that may be the key to understanding galaxy transformations, a point that will be discussed later on.

If one does happen to have distance measurements, many more properties can be measured since fluxes can be transformed into luminosities. Luminosities, in turn, can be used to compute, for example, stellar masses and star formation rates when used in conjunction with additional photometric information (e.g., colours). It is important to note that different filters are better proxies for different properties of galaxies. For example, infrared filters do a much better job of tracing stellar mass than, say, optical filters, since bright young stars do not have a substantial excess of infrared flux relative to the general stellar population (e.g. Bell & de Jong, 2001). Similarly, bright massive stars emit most of their radiation in the ultraviolet region of the spectrum, and are generally the only stars that do so. Since these stars do not live very long, their presence – as indicated by a UV detection – indicates that star formation has recently occurred (e.g., Hopkins et al., 2001). Therefore, it is important to employ a multi-wavelength approach whenever possible in order to glean as much information as possible.

Distances are most commonly measured with the *redshift*. A galaxy's spectrum is 'shifted' towards the red by the expansion of the Universe. By using

current cosmological parameters, it is a straightforward matter to transform the spectrum offset into a distance measure.

Obtaining distance measurements for large numbers of galaxies is a difficult and time-consuming task, and this has only been possible quite recently with advances in telescopes and survey technology. Therefore, it has become increasingly common to perform large-scale redshift surveys with the goal of beating down statistical uncertainties and cosmic variance, thus allowing a more complete understanding of the global properties of galaxies and galaxy populations. The largest survey to-date is the Sloan Digital Sky Survey (SDSS, York et al., 2000). The latest data release (Abazajian et al., 2009) contains photometry on over 350 million objects, of which almost a million galaxies have a measured redshift, with a median $z \sim 0.1$, which corresponds to a distance of ~ 400 Mpc. With such a massive dataset it is now possible to characterise in great detail the basic properties of nearby galaxies. For a thorough discussion on this topic, see Blanton & Moustakas (2009).

1.2 Galactic Environments

Observations of galaxies show that they tend to clump together over time. Structures in the Universe form hierarchically, and thus on average galaxies evolve from relatively isolated regions (often defined as the ‘field’) to more massive systems such as groups and clusters (e.g., White & Frenk, 1991; White & Rees, 1978). (To complicate matters, galaxies could also form in higher density environments to begin with, thus skipping the ‘field’ stage entirely.) Groups of galaxies are assemblages of three or more bright galaxies that are bound

(or will eventually become bound) to a common dark matter halo of mass $\sim 10^{13} M_{\odot}$, while clusters are generally regarded as groups on the scale of hundreds to thousands of galaxies, with masses $\gtrsim 10^{14} M_{\odot}$ (Sparke & Gallagher, 2007, Chap. 7). It is not surprising that such a buildup in density will have a non-negligible effect on the evolution of such galaxies. Indeed, field galaxies are generally found to be relatively blue, star-forming and disk-dominated, while those in clusters typically have redder colours (and thus older stellar populations), are mostly non-star-forming, and consist of a greater fraction of early-type morphologies (e.g., Postman & Geller, 1984; Balogh et al., 2007, 2009; Dressler et al., 1997). An understanding of how galaxies are transformed from disky and star-forming into old, red and ‘dead’ is a prime topic of research in galaxy evolution (e.g., Wilman et al., 2005a; Bower et al., 2006).

1.3 Observations of Environments and Interactions

Disentangling the evolutionary roles of a galaxy’s environment and its interactions with other galaxies is a question of nature versus nurture. Galaxies may form and progress through a series of natural environments throughout their lifetime, driven by the hierarchical build-up of mass as smaller dark matter haloes gradually merge into larger systems (e.g., Cole et al., 2000; Bower et al., 2006). Along the way, galaxies themselves might interact (‘nurture’) through mergers, collisions or may otherwise affect each other, sometimes in substantial ways (Ellison et al., 2008, 2010).

It has now been well-established that there is a universal trend for star formation to become suppressed in galaxies that are found in higher mass dark matter haloes (e.g., Lin et al., 2003; Gómez et al., 2003; Balogh et al., 2007). Alongside this correlation is that the ratio of dark-to-luminous matter content, otherwise known as the mass-to-light ratio (M/L), of galaxies and galaxy groups and clusters increases with increasing halo mass (e.g., Lin et al., 2004; Balogh et al., 2007; Eke et al., 2004a).

As hinted above, density is also seen to correlate with galaxy morphologies (Dressler, 1980). Lenticular galaxies become more common at moderate densities (Wilman et al., 2009) while ellipticals become more common at the highest densities (Postman & Geller, 1984). At higher densities, mergers are ever more likely, with the potential to distort these morphologies (e.g., Patton et al., 2002; Blaizot et al., 2006).

The overall effect is that galaxies that were once active and blue gradually fade onto a tight sequence of galaxies populating a red region of the colour-magnitude diagram (the ‘red sequence’, (Visvanathan & Sandage, 1977)) as quiescent, primarily bulge-dominated galaxies in high-density regions (McGee et al., 2008). However, precisely *what* processes affect the evolution of galaxies, and their relative importance, remain open questions (for a discussion of a more theoretical nature, see Bower & Balogh (2004)). Simply holding membership in a group or cluster might not be sufficient to drive all of these evolutionary processes. For example, Ellison et al. (2009) show that while galaxies within clusters have, on average, higher metallicities than their counterparts in the field, this trend is primarily correlated with local overdensity, and not cluster

membership. In addition, Balogh et al. (2004b) suggest that the galaxies that are star-forming evolve independently of their environment, dependent only on their intrinsic properties, at least for the present epoch. Therefore, while there are more star-forming galaxies in the field, their properties do not differ substantially from star-forming galaxies in clusters.

It is also unclear how important mergers and interactions are in the overall evolution of star formation rates in galaxies. Close pairs of galaxies are more likely to undergo, or to have undergone, a merger; thus, they are a very useful sample of interacting galaxies. In a study on galaxy pairs out to intermediate redshifts, Robaina et al. (2009) found that mergers may only trigger a relatively small fraction of star formation, at least since $z \sim 1$. However, there may be a dependence on morphology and environment in the efficiency of merger-triggered star formation (Moss & Whittle, 1993). Merger rates themselves are dependent on environment, where the slower relative motions of galaxies afforded in groups would be conducive to increased merger activity, while clusters' high velocity dispersions are less likely to promote merging (e.g., Athanassoula et al., 1997). Hence, properties of galaxies living in different environments, or galaxies in the process of merging, may be able to tell us something more concrete about their formation and evolution.

1.4 Galaxy Groups

When studying these evolutionary processes, it is useful to observe transformative steps. When is star formation shut down, exactly? Indeed, some theoretical (McGee et al., 2009) and observational (Balogh & McGee, 2010)

studies suggest that there is a ‘critical mass’ ($\sim 10^{13} M_{\odot}$) above which certain environment-driven effects (such as a truncation of star formation) are unlikely to occur. On the morphological aspect, Wilman et al. (2009) find that the fraction of S0 galaxies in groups is as high as in clusters (see also Quilis et al., 2000). What’s more, these galaxies are found preferentially in the outer regions of the groups, suggesting that they might arise from infalling spiral galaxies becoming stripped of their star-forming gas. Therefore, not only do galaxy groups lie between the field and clusters in terms of density, they may be the environment in which key evolutionary transformations take place. Galaxies in the nearby Universe reside most commonly in a group environment (Ramella et al., 1999; Eke et al., 2004b; Balogh et al., 2004a) and so understanding the properties of galaxy groups assists in our understanding of the current Universe as a whole.

1.5 Galactic Evolution Over Time

The above discussion centres on the description of galaxies in snapshots of time. Clearly, it is necessary to study the environmental and other effects over long periods of time, which provides another dimension of exploration in an effort to improve our understanding of the Universe. The way in which we can do this is to look at more distant objects, since their light will have travelled for a longer period of time before we detect it. Therefore, observing distant objects also means that we are observing the distant past. However, we cannot observe a single galaxy evolve over billions of years, but we can at

least statistically observe galaxies evolve by studying populations at different redshifts.

Observations of the distant Universe are, not surprisingly, more difficult. This is due to a number of factors. Distant objects:

- appear fainter, so they require deeper exposures,
- suffer from crowding, since the angular size of, say, a few kpc is smaller the further out we go, and
- have their light redshifted, so that a red filter may actually be detecting a bluer rest-frame flux.

Despite these difficulties, it is necessary to study the distant Universe in order to get a handle on galaxy evolution, and the evolution of the Universe as a whole.

With the above discussion in mind, a comparison of high-redshift and low-redshift studies does shed some light on how star formation, morphologies, colours, etcetera, of galaxies behave over large periods of time. The mass-to-light ratios of high- z galaxies show the same general trend with density as their low- z counterparts, but there seems to be little evolution beyond that which we would expect for a passively evolving population of stars (Balogh et al., 2007; Ramella et al., 2004). However, there does appear to be some evolution in the relative contributions of the disks and bulges in both group and field galaxies since $z \sim 0.4$, in that more distant groups have diskier galaxies than groups at low redshift, but that these disks are still suppressed relative to field galaxies (McGee et al., 2008). Despite the number of intermediate-redshift

works that have explored questions of galaxy evolution, going past $z \sim 1$ is even more difficult. Galaxies at these distances become very faint and closely-packed on the sky, and these issues will undoubtedly be the focus as ground- and space-based telescope technology advances.

1.6 Current Issues and Questions

While the studies discussed above are encouraging, they are not without issues. Simply finding galaxy groups to begin with is a difficult task. Massive clusters are relatively straightforward to spot with friends-of-friends algorithms (e.g., Carlberg et al., 2001; Eke et al., 2004b), as sites of X-ray emission (e.g., Ebeling et al., 2001), or significant overdensities of red sequence galaxies (Gladders & Yee, 2000). However, groups have low contrast relative to field galaxies, and extensive redshift surveys are generally required to implement a friends-of-friends algorithm to identify such galaxy associations. The difficulties do not stop there. Once groups are found, it is then necessary to determine which galaxies in one's photometric sample are actually members. This is usually done by placing reasonable constraints on transverse and line-of-sight distance. There are likely to be additional members of the group that cannot be assigned simply due to the limitations of the survey (e.g., photometric and spectroscopic limits, observing strategies). Often, it is necessary to correct for this incompleteness in a statistical way by, for instance, determining the fraction of galaxies for which redshifts were obtained as a function of apparent magnitude (e.g., Yee et al., 2000; Wilman et al., 2005b; Balogh et al., 2007, 2009). These methods introduce additional uncertainty in calculations

involving number counts (e.g. luminosity functions), so it is desirable to have as complete a survey as possible.

Having few member galaxies is a recurring problem in studies of galaxy groups. In almost all cases, the velocity dispersion of groups is used as a proxy for the total mass (including dark matter). This necessarily assumes that the system is in virial equilibrium, an assumption that is very likely incorrect for a large fraction of systems (McConnachie et al., 2008; Hou et al., 2009). Without a reasonably complete selection of the group members, it is challenging to determine reliable velocity dispersion measurements. By measuring mass using weak lensing, some assurance that the overall conclusions in our discussion are robust can be granted: both Hoekstra et al. (2001) and Parker et al. (2005) find that the lensing masses of stacked groups are consistent with the virial masses of the same groups. While weak lensing has its own shortcomings – it is sensitive to the total projected mass in the angular field of view and requires a stacked measurement due to the weak signal – the uncertainties in weak lensing are completely independent of the dynamical methods of halo mass measurement. In addition to uncertainties in velocity dispersion, statistical variation due to the identification of few members becomes troublesome, especially for more distant groups. Not only do galaxies become more closely packed in a telescope’s field of view, fainter objects become very difficult to detect as the distance of the group increases; this is especially true for spectroscopic measurements, where it can be difficult to reconcile priorities to determine an appropriate slit design – targets might have to be awkwardly spaced and often ranked in priority based upon brightness. The best way to

counter these issues is to re-observe the same fields multiple times in an effort to obtain redshifts for everything down to the photometric limit.

Clearly, it is inevitable that low-redshift studies will be able to probe down to lower luminosity (i.e. faint) galaxies than studies at higher redshift. This leaves the faint end of galaxies relatively unexplored. However, these faint galaxies can harbour some of the most interesting science. For instance, it has been shown that the shutdown in star formation across the history of the Universe is preferentially affecting higher-mass galaxies so that the lowset-mass galaxies are the only source of significant star formation at the present day. This phenomenon is commonly referred to as ‘cosmic downsizing’ (e.g., Cowie et al., 1996; Heavens et al., 2004; Juneau et al., 2005).

1.7 Thesis Objectives

In view of the above, this thesis aims to improve the membership statistics of intermediate redshift groups and, in so doing, explore the properties of the faintest members of these galaxy groups. This will be accomplished using new spectroscopic observations of ten groups selected around $z \sim 0.4$. The observations were designed specifically to focus on galaxies fainter than the original survey’s spectroscopic limit of $R = 21.5$, to probe much fainter, down to $R = 23.25$. These data are augmented by previous follow-up spectroscopy that probed down to a statistical completeness limit of $R = 22$. We thus have a sample of group galaxies with luminosities spanning a range among the widest yet studied at intermediate redshift.

In this thesis, we will first present in §2 a description of the GEEC galaxy sample, highlighting the extensive multi-wavelength observations conducted to-date. We will then discuss our additional spectroscopic observations from FORS2 and data reduction techniques, including redshift determination. Our methodology for the calculation of group properties and results are described in §3. We present a comparative discussion in §4, and give a summary of our main conclusions and remarks on future work in §5.

Throughout this work we adopt a cosmology in which $\Omega_\Lambda = 0.7$, $\Omega_m = 0.3$ and $h = 0.7$.

Chapter 2

The Data

2.1 The GEEC Galaxies

Our Group Environment and Evolution Collaboration (GEEC) utilises an extensive dataset of multiwavelength photometry and a series of spectroscopic observations. The GEEC project is a follow-up from a previous survey, referred to as the second Canadian Network for Observational Cosmology (CNOC2) redshift survey (Yee et al., 2000). The survey covers about $\sim 1.5 \text{ deg}^2$ over four separate patches, which helps to mitigate biases that might be introduced due to cosmic variance. Two of these patches are shown in Figs. 2.1 and 2.2. Original photometry was obtained from the Canada-France-Hawaii telescope (CFHT) in the U , B , V , R_c and I bands. With the CFHT's multi-object spectrometer, approximately 6000 redshifts were obtained, mostly for the brighter objects; about 50 per cent of objects down to $R = 21.5$ have a measured redshift. This completeness is primarily dependent on apparent magnitude, a point which will be discussed in detail in §3.

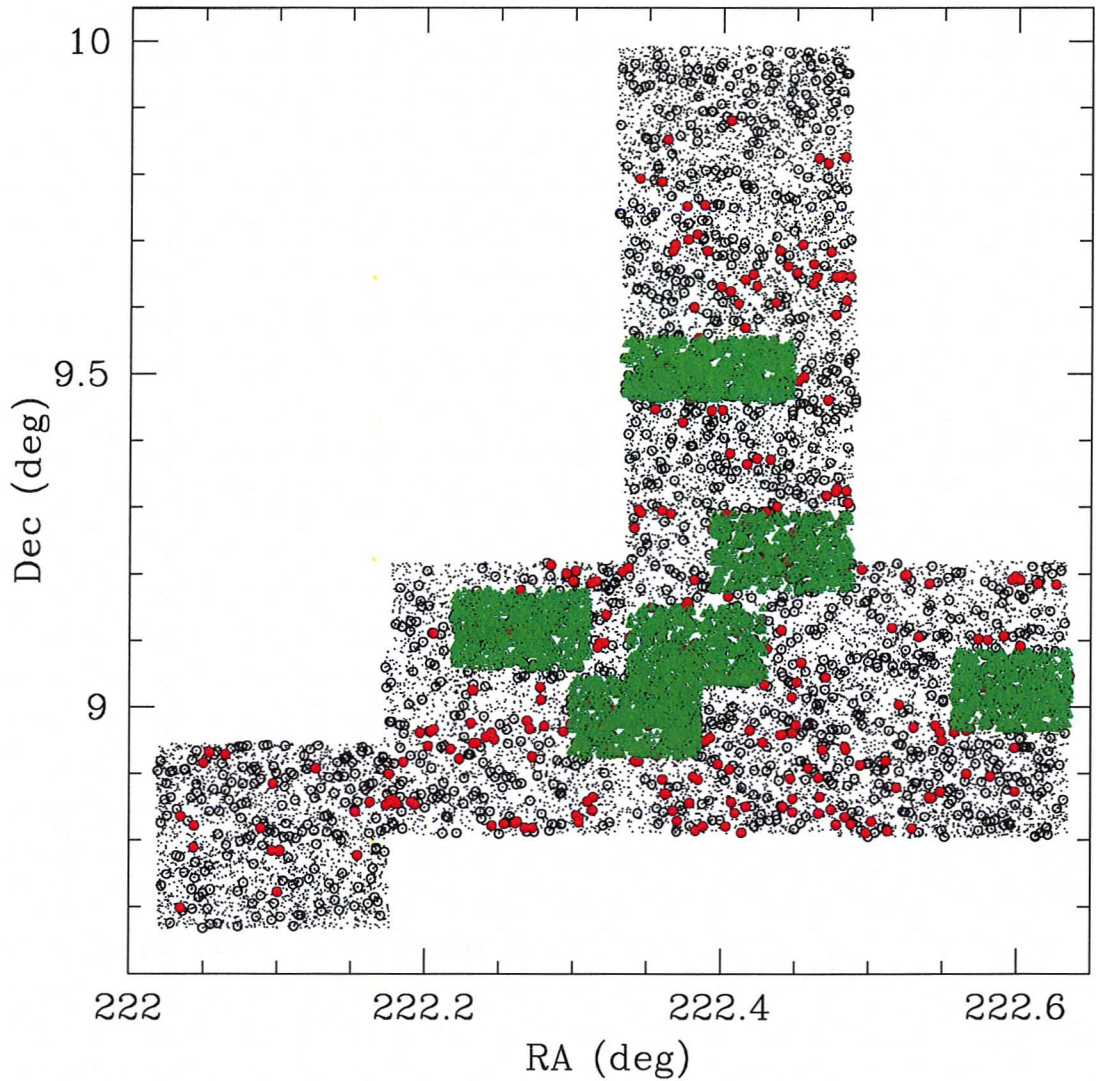


Figure 2.1: The CNOC2 14hr field. Filled red symbols indicate group galaxies, and the circles are galaxies with a previously-measured redshift. Green rectangles are the FORS2 target fields. Points indicate the entire photometric sample.

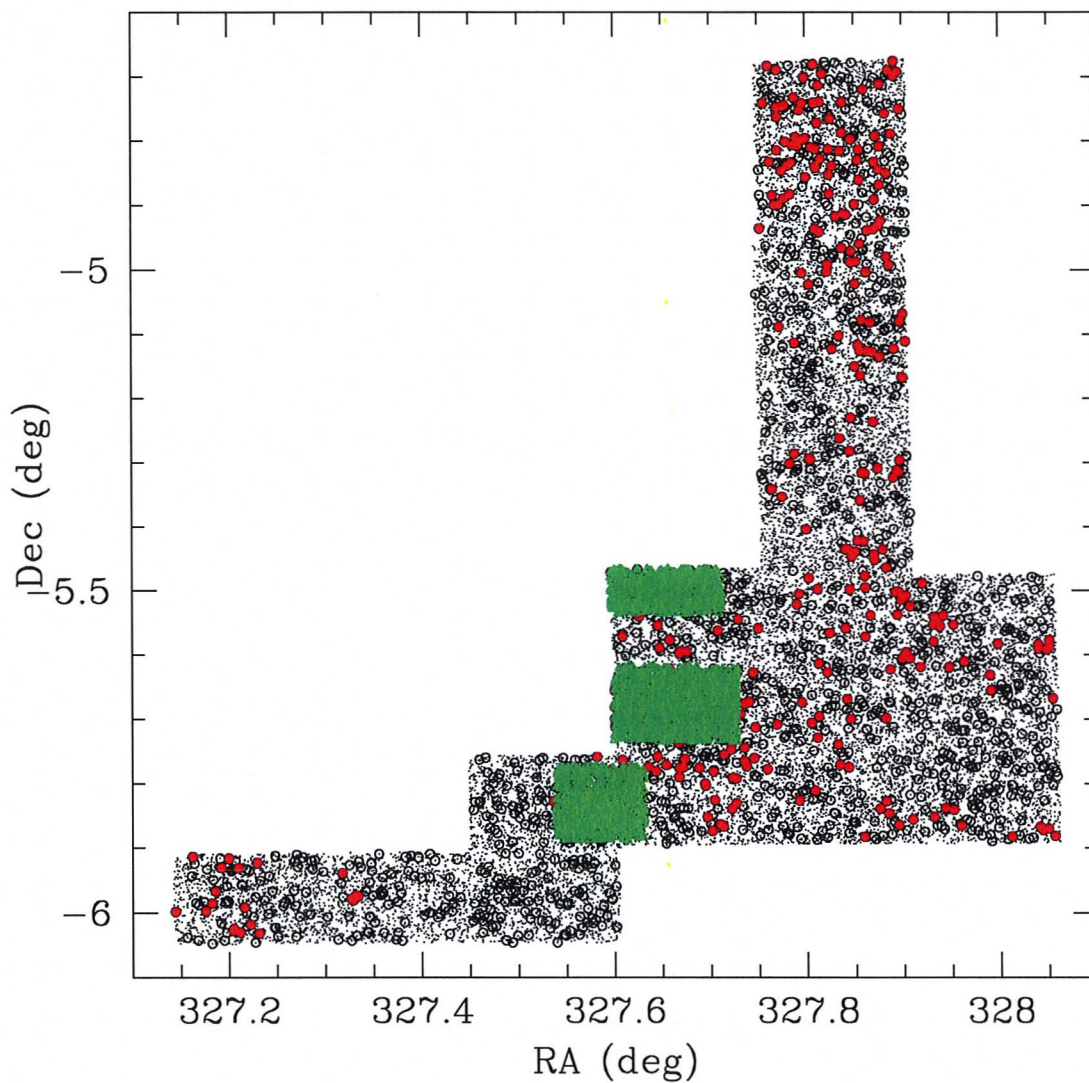


Figure 2.2: The CNOC2 21hr field. Symbols are as in Fig. 2.1.

Galaxy groups within these initial observations were identified by Carlberg et al. (2001) using an iterative friends-of-friends algorithm (e.g., Huchra & Geller, 1982). In brief, this method selects a galaxy at random to form a trial group, and locates galaxies within a specified 3D distance (the galaxy’s ‘friends’) based upon the angular positions of the other galaxies and their relative radial velocities. (The ‘line-of-sight’ distance between two galaxies was measured relative to the group centre as $c(z - z_{\text{grp}})$.) Galaxies near to the friends are then located (the ‘friends’ of the friends). This process is iterated until the group stabilises. In general, only groups having greater than three members (each above a specified luminosity limit) are kept. It is also possible to adjust the algorithm’s parameters for more specialised group-finding (e.g. compact groups).

Over 200 systems at intermediate redshift ($0.1 < z < 0.55$) were found in the CNOC2 galaxy sample by Carlberg et al. (2001). After additional spectroscopic observations (see below), groups were re-identified by Balogh et al. (2007) following the work of Wilman et al. (2005b). In this procedure, members were added to the existing groups based upon a cut in projected distance and line-of-sight velocity that depends upon the velocity dispersion and distance of the group. Using these member galaxies, the velocity dispersion and luminosity-weighted centres were recomputed. New members were then added or deleted accordingly. The process was repeated until a stable group membership was established, which generally occurred within two to four iterations. This method, applied to the CNOC2 survey, forms the current GEEC galaxy group sample. We will now discuss details of the photometric and spectroscopic observations of this survey.

2.2 Photometry

Recently, Balogh et al. (2009) presented a detailed photometric analysis of GEEC galaxies, compiling near-IR data from the *William Herschel Telescope* (WHT), *New Technology Telescope* (NTT), and archival *Spitzer* IRAC data, combining these with our previous follow-up CHF12K observations and archival Megacam data from CFHT.

The irregular geometry of the CNOC2 patches (as seen in Figs. 2.1 and 2.2) made follow-up observations difficult to achieve in a uniform manner. In Balogh et al. (2009), all of the images were PSF matched for optimal photometry, and calibrated using either 2MASS (Jarrett et al., 2000) (for the NIR data) or with overlapping SDSS images (for the optical data). Actual object detection was performed using SExtractor v2.5 (Bertin & Arnouts, 1996). Both 3" and 5" aperture magnitudes were computed, and here we adopt the 3" magnitudes for our analyses. There is no indication of systematic biases between colours measured from either aperture (Balogh et al., 2009), and in fact the smaller apertures are more useful to avoid biases from galaxies with close companions. The larger aperture magnitudes are useful for IR and Galex UV data, where the PSF is larger than the optical.

2.2.1 Other Sources

2.2.1.1 GALEX UV Data

Recently, our collaboration was awarded 9 orbits of GALEX¹ UV observations, and data were obtained for 3 of the 4 patches (2hr, 14hr and 21hr) totalling ~ 13.5 ks in exposure time. The 1.25 deg diameter pointings targetted the centres of the main (square) portions of the patches. Therefore, coverage is not complete for all of the GEEC data. The use of ultraviolet data allows a measurement of star formation rates (SFR), given that massive, hot stars emit strongly in this waveband. The effects of dust can be addressed by deriving the SFRs from a fit to the galaxies' SEDs afforded by the extensive multiwavelength data available to the GEEC sample. Such an analysis will be presented in McGee, S. et al. (in preparation).

2.2.1.2 MIPS 24 Micron Data

We also have observations from the MIPS instrument on-board the Spitzer Space Telescope (Rieke et al., 2004), targetting the regions containing LDSS2 follow-up spectroscopy. In these targetted groups, and within our redshift range of interest, 79 group galaxies and 65 field galaxies were detected with MIPS, and the remaining 232 group galaxies and 236 field galaxies received upper limits on their 24 μ m flux. Analysis and results from these data will be presented in Tyler, K. et al. (in preparation).

¹ Space observatory web page: <http://www.galex.caltech.edu/index.html>

2.2.1.3 X-ray Observations

Two of our patches (the 14hr and 21hr) were observed with Chandra and XMM-Newton and reported in Finoguenov et al. (2009). Some of the groups in the GEEC sample correlate well with X-ray detections, while many do not. There also does not appear to be a clear correlation between the dynamical state of our groups and their detection in X-ray (see Hou et al., 2009; Finoguenov et al., 2009). A detailed comparison of the properties of groups detected with optical observations versus X-ray will be presented in a future GEEC paper (Connelly, J. et al., in preparation).

2.3 Previous Follow-up Spectroscopy

Wilman et al. (2005b) targetted 20 of the GEEC groups with the second Low Dispersion Survey Spectrograph (LDSS2) on the Baade telescope at Las Campanas Observatory in Chile. All of the groups in our current work were present in these LDSS2 observations. This survey was able to correct for incompleteness down to $R = 22$, slightly deeper than the original CNOC2 sample, which was limited to $R = 21.5$. We aim to improve the completeness and depth of observations of our targetted groups by combining these data with new spectroscopy, which we describe below.

2.4 Observations and Data Reduction

New spectroscopic observations of 10 GEEC groups were obtained from the FOcal Reducer/low dispersion Spectrograph 2 (FORS2) instrument on

the Very Large Telescope (VLT). These groups were selected specifically from the high- z end of our entire sample to facilitate a study on evolution. Six of the groups are in the 14h field, and 4 are in the 21h field. Basic data on the observations and groups are shown in Table 2.1, and the distribution of the group velocity dispersions with redshift is shown in Fig. 2.3.

Over the course of several nights in June through August, 2005, spectra were taken of approximately 500 galaxies in 10 masks targetting the GEEC groups. Exposure times of individual frames ranged from 2390 to 3230 seconds, with 3 exposures per mask. The instrument consists of two adjacent CCDs ('chips') per mask. We used the instrument grism GRIS_300V+20 with the GG375 order separation filter, giving a wavelength range of 385-750nm. With this setup, the dispersion is $111\text{\AA}/\text{mm}$. The standard resolution collimator was used, giving an angular resolution of 0.25 arcsec / px , with a corresponding field of view of $6.8' \times 6.8'$.

Our raw science exposures were first combined to create single master frames for each group. Each chip was treated separately through the entire data reduction procedure, as they require different bias and flat field corrections.

On some occasions, all science exposures were not taken on the same night. In these cases, we use the first night's calibration frames in the beginning stages of reduction. This is not much of a concern since there is little variation between adjacent nights. However, for one of the 21hr groups (138), a third exposure was taken many days after the first two. In this case, we do not use the third exposure because the calibration images are not applicable. This

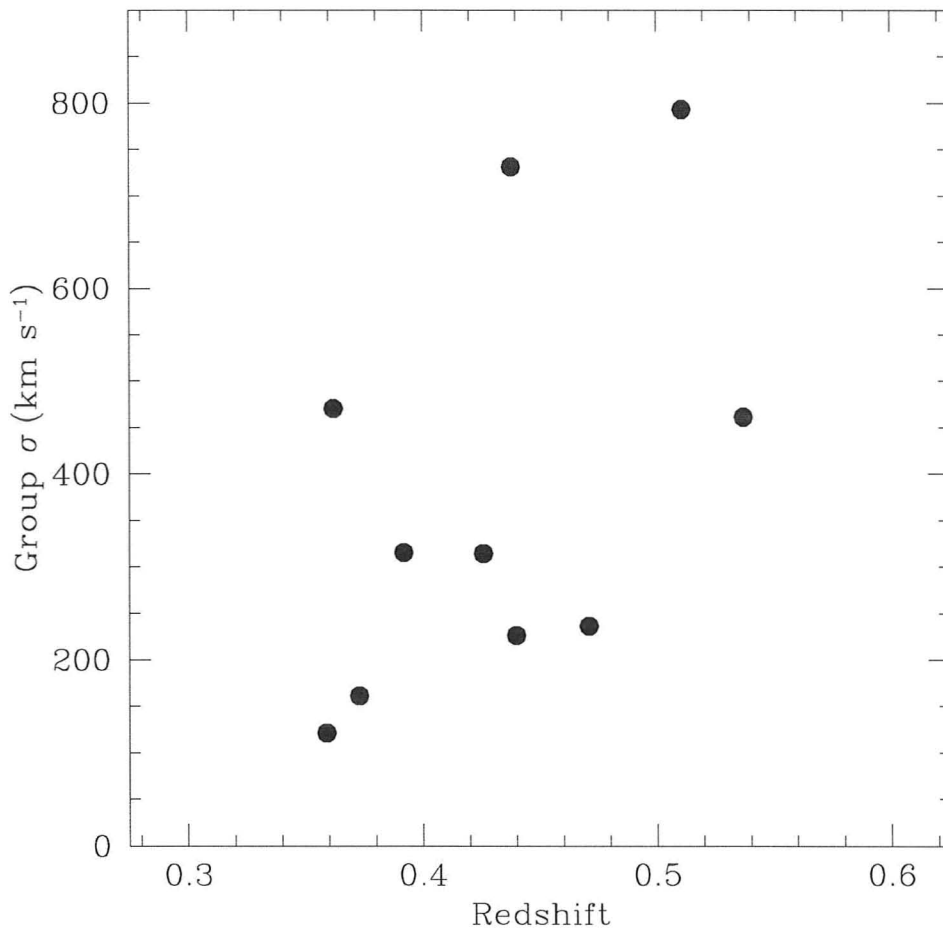


Figure 2.3: Group sample intrinsic velocity dispersions plotted against redshift. These 10 groups in our targetted sample are restricted to $0.35 < z_{\text{grp}} < 0.55$. Eight of the groups scatter closely about $z = 0.4$.

Table 2.1: Basic data on our GEEC group sample. In the columns are the group IDs, the redshifts of the groups, positions, velocity dispersions, number of previously-existing members, and the number of newly-added members exclusively from the additional FORS2 data.

| Group ID | z | RA (J2000) | Dec (J2000) | $\sigma / (km\ s^{-1})$ | $N_{\text{mem}}^{\text{prev}}$ | $N_{\text{mem}}^{\text{new}}$ |
|------------|-------|------------|-------------|-------------------------|--------------------------------|-------------------------------|
| 14hr Field | | | | | | |
| 24 | 0.359 | 14:49:03.9 | +09:06:57 | < 121 | 12 | +3 |
| 25 | 0.362 | 14:49:40.8 | +09:13:43 | 470 | 17 | +3 |
| 28 | 0.373 | 14:50:22.8 | +09:01:13 | 161 | 6 | +1 |
| 37 | 0.471 | 14:49:29.1 | +09:05:33 | 236 | 13 | +9 |
| 38 | 0.511 | 14:49:27.8 | +08:58:12 | 773 | 18 | +3 |
| 39 | 0.537 | 14:49:23.2 | +09:30:24 | 461 | 12 | +7 |
| 21hr Field | | | | | | |
| 134 | 0.392 | 21:50:24.8 | -05:41:29 | 315 | 11 | +2 |
| 137 | 0.426 | 21:50:37.7 | -05:29:18 | 314 | 8 | +2 |
| 138 | 0.438 | 21:50:48.2 | -05:39:53 | 730 | 30 | +18 |
| 139 | 0.440 | 21:50:25.8 | -05:50:20 | 231 | 9 | +4 |

reduction method, involving combined science frames before reduction, is preferred so that the data are compatible with the redshift determination code (see below).

We used the FORS2 data reduction pipeline² to calibrate and reduce the spectroscopy. Master calibration frames and tables (e.g., slit locations) were produced using the program ESOREX data reduction recipe *fors_calib*, from five bias frames, three flat fields, one arc lamp exposure and information about the instrument grism. The calibration products (e.g., master bias and flat field) were then used to reduce the science frames and produce the final data products. This final step was performed with the recipe *fors_science* using the same program. The data reduction products that are directly used in the redshift determination (discussed below) are:

- a 2D image of reduced, sky-subtracted 2D spectra,
- the primary reduced 2D image containing the 1D sky-subtracted spectra, 1 per row of pixels, in which the 2D counterparts have been summed along the y-axis,
- a noise map of the spectra and
- the object table, containing a list of the objects successfully extracted from the raw data.

² Information on the VLT, FORS2 and its data reduction pipeline software can be obtained from the instrument web page: <http://www.eso.org/sci/facilities/paranal/instruments/fors/>

2.4.1 Redshift Determination

Extracted spectra from our calibrated and reduced observations were cross-correlated with a library of templates using ZSPEC, an IDL script written by Renbin Yan. The program has an efficient graphical interface. The user may observe fits to template spectra from a ranked list of most probable redshifts, and compare them directly with the data. Use of these interactive steps helps to avoid matching to sky lines, as we discuss below.

Since our FORS2 data are not identical to the type of observations for which ZSPEC was designed, it was necessary to adapt our sky-subtracted spectra to the program's requirements. This consisted of padding the spectra with null pixels for consistent wavelength coverage and recomputing the noise. For the latter, this involved downweighting the tail ends of the spectrum so that the templates are not convolved with low-signal regions. Each spectrum was then processed with ZSPEC and analysed for redshift identification.

Before discussing the results of processing through ZSPEC, we note that the *iraf* routine XCSAO, used for radial velocity determination, was explored as an option for redshift-finding. While this code is quick, it has a limited library of templates and no interactive graphical interface with which to actively participate in the selection of redshifts. Generally, this code works well for spectra with strong features, but lacks accuracy for weakly-featured spectra. Hence, the interactivity of ZSPEC is far more efficient for our task, which involves very faint targets, many of which lack strong emission lines.

Each of the ~ 500 spectra were plotted and compared with the best-fitting template along with the sky spectrum. In Fig. 2.4 there is a screenshot of the

program's interface. A large library of templates is available for use in ZSPEC, including emission-line and absorption-line galaxies, QSOs, and stars. Careful consideration was made to avoid features overlapping with sky emission. When necessary, the 2D spectra were consulted to support the presence (or absence) of a real emission line (e.g., OII): sky lines will appear along the entire length of the slits but emission lines appear as bright spots where most of the galaxy's light falls. Quality flags were assigned on a scale of 1 to 4, with 4 being the highest confidence (3 is very good, 2 generally indicates weak features or absorption only, and 1 is poor). Galaxies at a quality level of zero (no redshift) are retained only for the purposes of determining FORS2 coverage and success rates. Fig. 2.5 shows an example of randomly-selected spectra for each of the levels of quality.

In Fig. 2.6 we show the success rate of our redshift-finding algorithm. In bins of apparent r (aperture) magnitude, the histograms represent the total number of target spectra extracted from the data (solid line) and the number of successful redshifts in that bin (dashed line). For later comparison, we also show a histogram of the number of new group members in each bin of apparent magnitude (dotted line). Success rate as a percentage is shown as points.

To determine an uncertainty for our new redshifts, we use a small number of galaxies common to both the FORS2 and CNOC2/LDSS2 redshift samples. In Fig. 2.7 we show the rest-frame difference between the measured redshifts for these galaxies, symbol-coded for their origin (CNOC2 or LDSS2). Our redshift range of interest for this work is $0.3 < z < 0.6$ given our group sample (see Table 2.1), and so if we restrict the common sample galaxies to

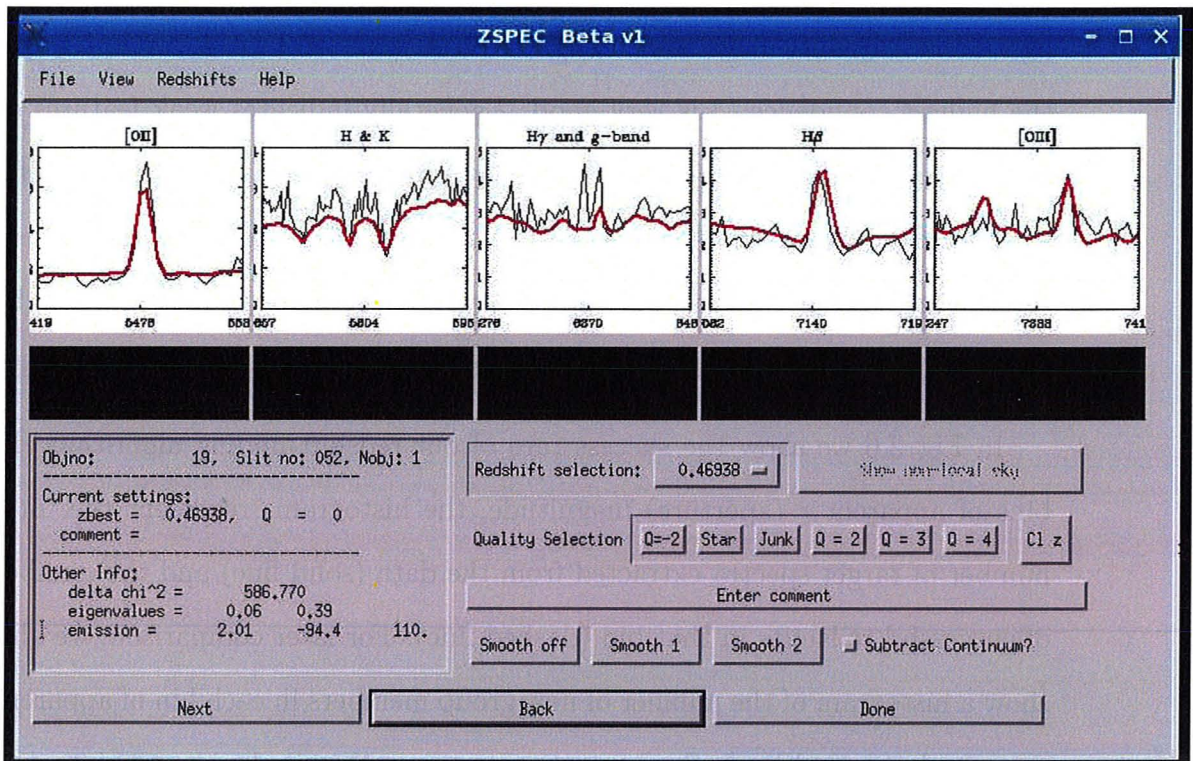


Figure 2.4: An example spectrum as it appears on the ZSPEC interface. This spectrum's fit is clearly of high quality.

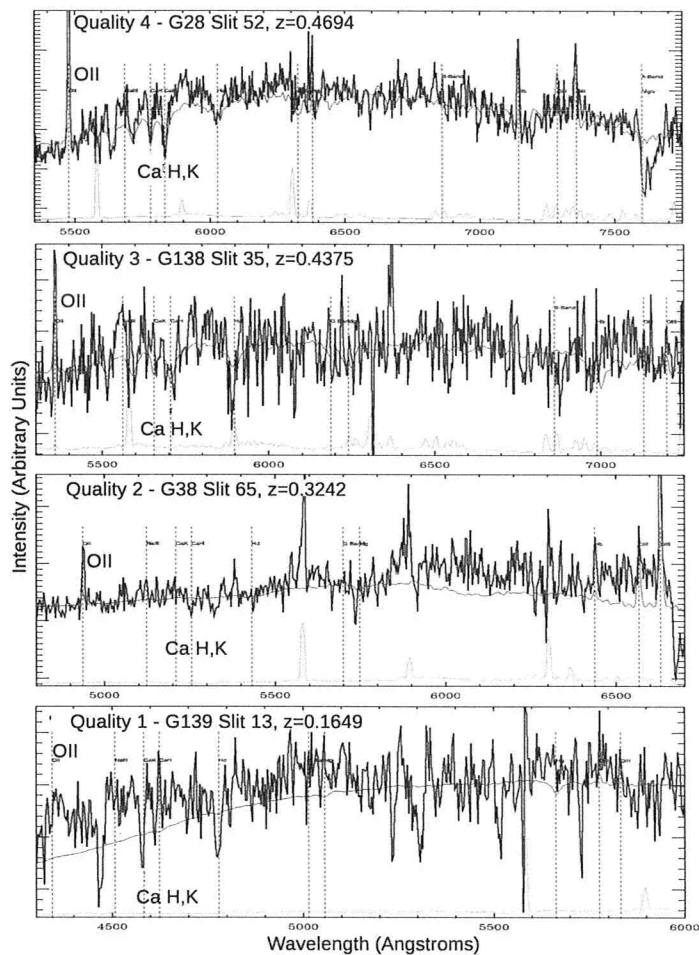


Figure 2.5: Randomly-selected example spectra from each redshift quality class. The highest quality (4) is at the top. Each best-fitting redshift is shown, with the template as the thin red line. A typical sky spectrum is shown in turquoise. The most prominent spectral features that were used to determine z are labelled (OII, Ca H & K). Vertical dashed lines should be disregarded as a by-product of the program output. Also, we note that the spectra become congested with sky emission redwards of about 6500 angstroms.

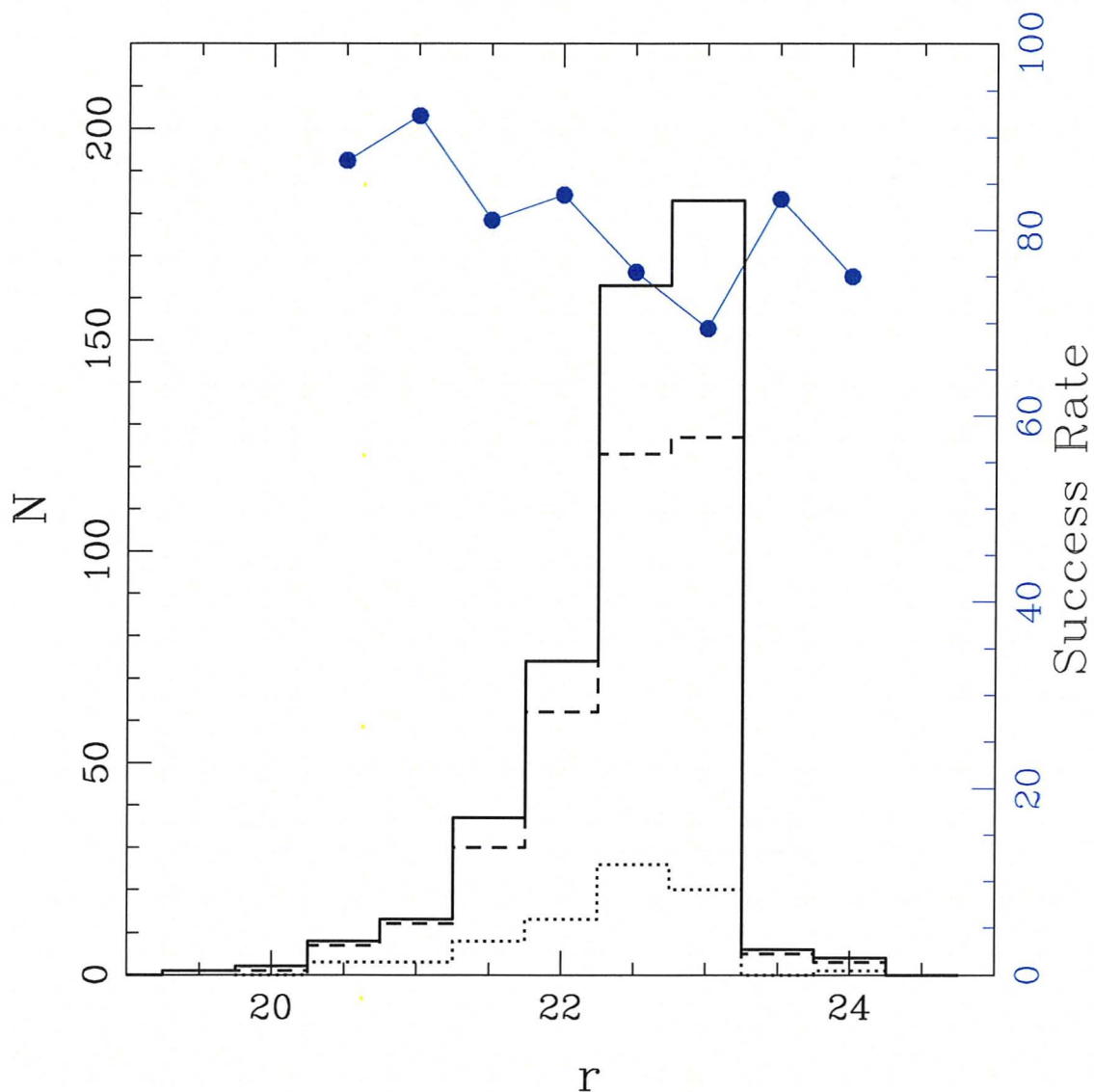


Figure 2.6: Success rate of our FORS2 target sample in bins of apparent r magnitude. The solid histogram shows targets with extracted spectra, and the dashed histogram indicates the number of successful redshifts. For comparative purposes, counts of new group members are shown in the dotted histogram. The points are the success rate as a percentage, based on the right-hand axis.

that range we get an overall mean and standard deviation of 9.6 km s^{-1} and 149 km s^{-1} , respectively. Yee et al. (2000) showed their uncertainty to be 103 km s^{-1} for the original survey, and Wilman et al. (2005b) found an uncertainty of 142 km s^{-1} for the LDSS2 galaxies. Splitting our common sample into those from CNOC2 and LDSS2, our mean and standard deviation for each of those are, respectively: 28 km s^{-1} and 143 km s^{-1} (CNOC2); -22 km s^{-1} and 165 km s^{-1} (LDSS2). Given the uncertainty of each sample's CNOC2 or LDSS2 redshifts, we can compute an uncertainty in our sample that is derived from both of these as follows. For CNOC2, the uncertainty in our redshifts is then $\sqrt{143^2 - 103^2} = 99 \text{ km s}^{-1}$. Similarly, for the LDSS2 sample we get $\sqrt{165^2 - 142^2} = 84 \text{ km s}^{-1}$. Finally, we will take the average of these two values: 92 km s^{-1} . Therefore, we adopt an uncertainty of 92 km s^{-1} in our measured redshifts.

2.5 Summary of the Data

Bringing together the various sources of data discussed above, we now have a sample of group and field galaxies from 10 target fields of the FORS2 instrument. Our data consist of multiwavelength, well-calibrated photometry, plus spectroscopy (redshifts) from the original CNOC2 survey and previous follow-up observations from LDSS2 that are provide a useful sample of galaxies down to a magnitude limit of $R = 22$. The new FORS2 data then extend the above sample of galaxies down to a magnitude limit of $R = 23.25$.

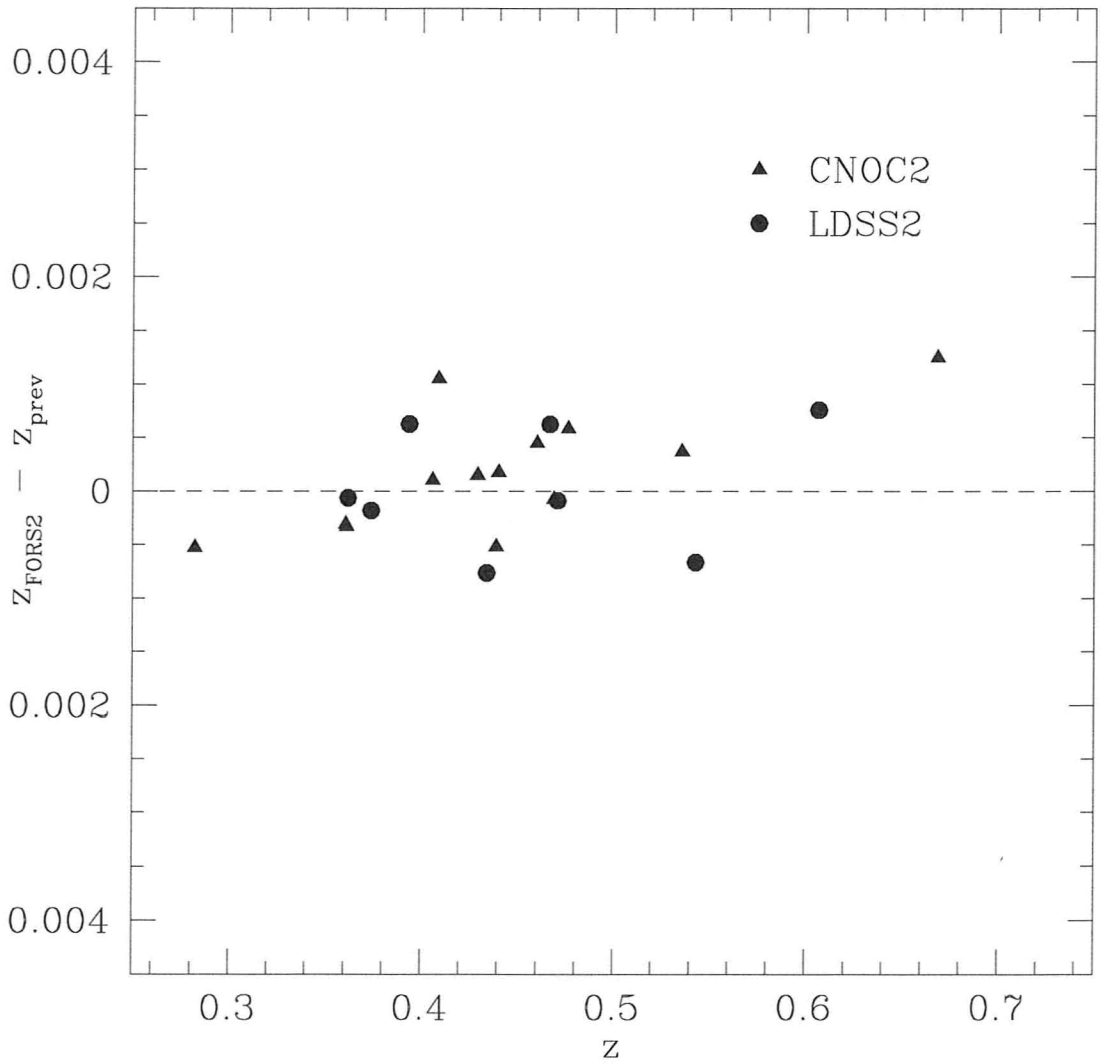


Figure 2.7: Comparison of a small number of galaxies common to both the FORS2 and CNOC2 or Magellan LDSS2 samples. Differences in their redshifts are shown as a function of redshift. The standard deviation is 149 km s^{-1} .

Chapter 3

Analysis and Results

3.1 Galaxy Group Membership

With our data in-hand, it is then necessary to construct samples of group and field galaxies. While the groups themselves were initially found by Carlberg et al. (2001), with additional spectroscopy we must assign the new galaxies as either members of one of these groups, or not. In the latter case, the galaxy is assigned to our ‘field’ sample. It is possible to re-define the group centres and velocity dispersions to re-compute the membership entirely; however, as we will see in §4.2, the velocity dispersions do not change significantly, and the luminosity-weighted group centres are unlikely to be altered due to the low luminosity of these new galaxies. Therefore, we will defer this procedure to future work where the entire catalogue will be subjected to a complete re-run of our FOF algorithm.

Defining angular and line-of-sight distances out to which a galaxy is defined to be within a group can be a difficult process. While our group sample may be largely non-virialised (Hou et al., 2009), it has been shown that estimates

of their mass based upon their velocity dispersions are statistically consistent with their lensing masses (Parker et al., 2005; Balogh et al., 2007); therefore, using radial and line-of-sight velocity (redshift) cuts derived from the groups' velocity dispersions is reasonable, at least in the absence of more detailed information on the individual groups.

Transforming the velocity dispersion into measurements of group size is usually done by defining a sphere of some radius that encloses a specified density relative to some benchmark. One such definition is R_{200} (e.g., Carlberg et al., 1997), which is the radius enclosing an overdensity equivalent to 200 times the critical density of the Universe at that redshift. This radius is, in turn, defined in terms of the group velocity dispersion, which can also be used to compute the virial mass of the group (which assumes that the group is in virial equilibrium).¹ The virial radius R_{200} can be expressed as

$$R_{200} = \frac{\sqrt{3}\sigma}{10H_0(z)(1+z)^{1.5}}, \quad (3.1)$$

in which $H_0(z)$ is the Hubble constant at redshift z and σ is the group velocity dispersion (e.g., Carlberg et al., 1997).

We show in Fig. 3.1 the differences between the velocities of each galaxy and its potential host group velocities, normalised by the group velocity dispersion, plotted against the distance from that group. For the purposes of our analysis, we consider galaxies to be group members if they are within a line-of-sight velocity of $\pm 3\sigma$ and, following Wilman et al. (2005b), within 1 Mpc of the

¹ Groups are not necessarily in virial equilibrium, so this procedure calculates properties (e.g., radius, mass) *as if the group were in virial equilibrium*.

group centroid. Therefore, group galaxies are scattered in the region defined by ± 3 in the vertical axis in Fig. 3.1 and within 1 Mpc radius. We will explore how our results are affected by this choice in radial cut in §4.

3.2 Completeness Corrections

Ideally, one would be able to obtain spectroscopy for every galaxy in our photometric sample, so that analyses can be performed without bias. Spectroscopic observations are expensive and time-consuming, and prioritisation of targets must occur. As a result, the targets most likely to be successful are chosen first – these are, usually, the brightest. While the observations undertaken for this work aim to probe fainter galaxies, the number of targets increases sharply the fainter we go, and there still is a significant fraction of unobserved targets in the magnitude range of interest. Therefore, we must correct for the fact that we simply do not have redshifts for everything. Otherwise, we will not be fairly extrapolating the results we would obtain had the redshift survey been complete.

As previously discussed, the original CNOC2 redshift survey consisted of spectroscopy on roughly half of the galaxies down to $R = 21.5$. Yee et al. (2000) presented a weighting scheme that depended on the geometry of the masks (since the placement of slits is not uniform) as well as magnitude, in an attempt to account for incomplete sampling in different masks. In this way, statistical completeness was achieved for the galaxies down to the spectroscopic magnitude limit of $R = 21.5$.

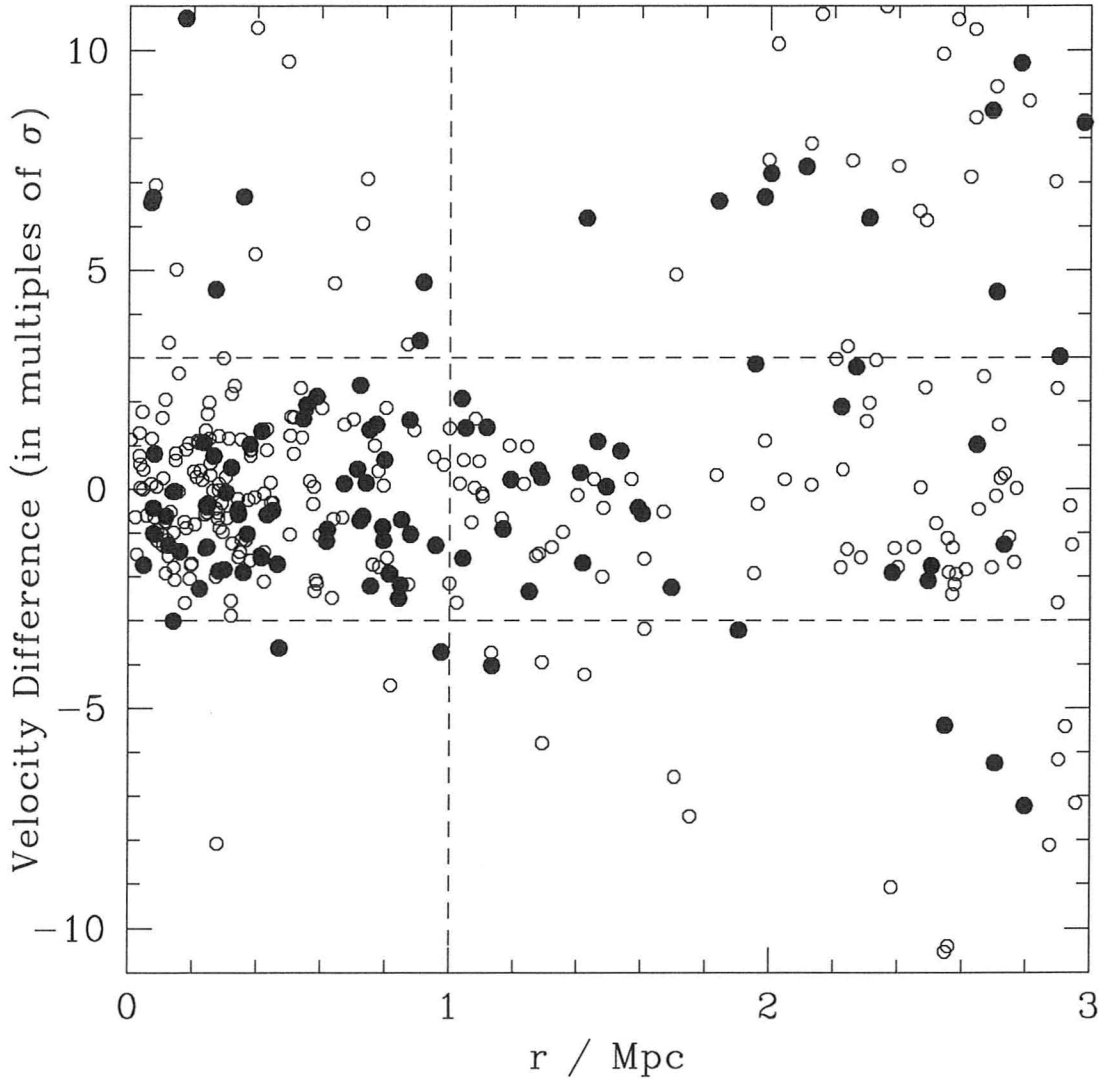


Figure 3.1: Velocity differences of our sample of galaxies, computed as the difference between the galaxy redshift and the redshift of our groups. All galaxies within 3 Mpc of any given group are included in this figure, and thus they may appear more than once. Empty circles are all galaxies in the CNOC2 and LDSS2 samples, and those that are filled are new FORS2 objects. Our group members are clustered in the region bounded by $r \leq 1\text{Mpc}$ and $\pm 3\sigma$.

With extensions to the original data from Magellan (to $R = 22$), various other weighting schemes were employed to correct for incompleteness down to the Magellan limit. The first of these weights were computed by Wilman et al. (2005b), where corrections were made individually to the target fields based on apparent R magnitude and the galaxies' radial positions from the target group centroids. Part of the motivation behind this method is that richer groups are more likely to be sampled incompletely due to their higher density of galaxies, and the relatively constant density, for all groups, at which we can take spectra with a given mask design. However, Balogh et al. (2007) measured weights based upon magnitude only for three bins of group velocity dispersion, and found that incompleteness is only about 10 per cent greater than the average for the richest groups. In a more recent paper, Balogh et al. (2009) simply chose to apply weights based on apparent magnitude, with no dependence on position or group richness. While applying weights is important for meaningful results, Balogh et al. (2009) point out that results in all of the above weighting schemes are negligibly affected by the choice of a particular weighting scheme.

Therefore, we adopt the magnitude-dependent weighting scheme of Balogh et al. (2009). In that work, all of the galaxies were divided into two samples, one where there is follow-up (Magellan LDSS2) spectroscopy (their $R \leq 22$ sample) and one where there is not (their $R \leq 21.5$ sample). The original CNOC2 (successful) redshift sample is biased toward strong emission line galaxies (since these are the easiest for which we can obtain a redshift), so it is also necessary to correct for this targetting bias. The final weight applied to each galaxy as applied by Balogh et al. (2009) is given in Wilman et al.

(2005b), for the CNOC2 and Magellan samples, respectively, without radial weights:

$$W_{\text{mag}}^{\text{CNOC2}} = 1 + \frac{\{N_{\text{phot}} - N_{\text{CNOC2},z} - N_{\text{LDSS2},z}\}}{N_{\text{phot}}} \quad (3.2)$$

$$= 1 + [1 - S_{\text{mag}}^{\text{CNOC2},z} - S_{\text{mag}}^{\text{LDSS2},z}] \quad (3.3)$$

$$W_{\text{mag}}^{\text{LDSS2}} = 1 + \frac{\{N_{\text{phot}} - N_{\text{CNOC2},z} - N_{\text{LDSS2},z}\}}{N_{\text{phot}}} \frac{N_{\text{phot}} - N_{\text{CNOC2},z}}{N_{\text{LDSS2},z}} \quad (3.4)$$

$$= 1 + [1 - S_{\text{mag}}^{\text{CNOC2},z} - S_{\text{mag}}^{\text{LDSS2},z}] \frac{1 - S_{\text{mag}}^{\text{CNOC2},z}}{S_{\text{mag}}^{\text{LDSS2},z}} \quad (3.5)$$

where the S_{mag} functions represent the selection functions of each sample – the fraction of galaxies with a measured redshift. For this work, we have a second follow-up redshift sample to add. All 10 of our targetted groups have Magellan spectroscopy, and they are each unbiased in colour, so we combine the samples and treat them as one follow-up sample as above (i.e., the LDSS2 sample above is now composed of both the LDSS2 and FORS2 redshifts). The results of this are shown in Fig. 3.2. Finally, we limit the CNOC2 sample to a magnitude of $R = 22$ and assume that, with the additional spectroscopy, we are able to correct for targetting bias and completeness up to this limit (Wilman et al., 2005b). As we will see, the FORS2 sample is unbiased in terms of target selection (as was the LDSS2 sample, see Wilman et al. (2005b)), so the only limit that we need to consider is a cutoff based upon the quality of the photometric data at the faint magnitudes (see next section).

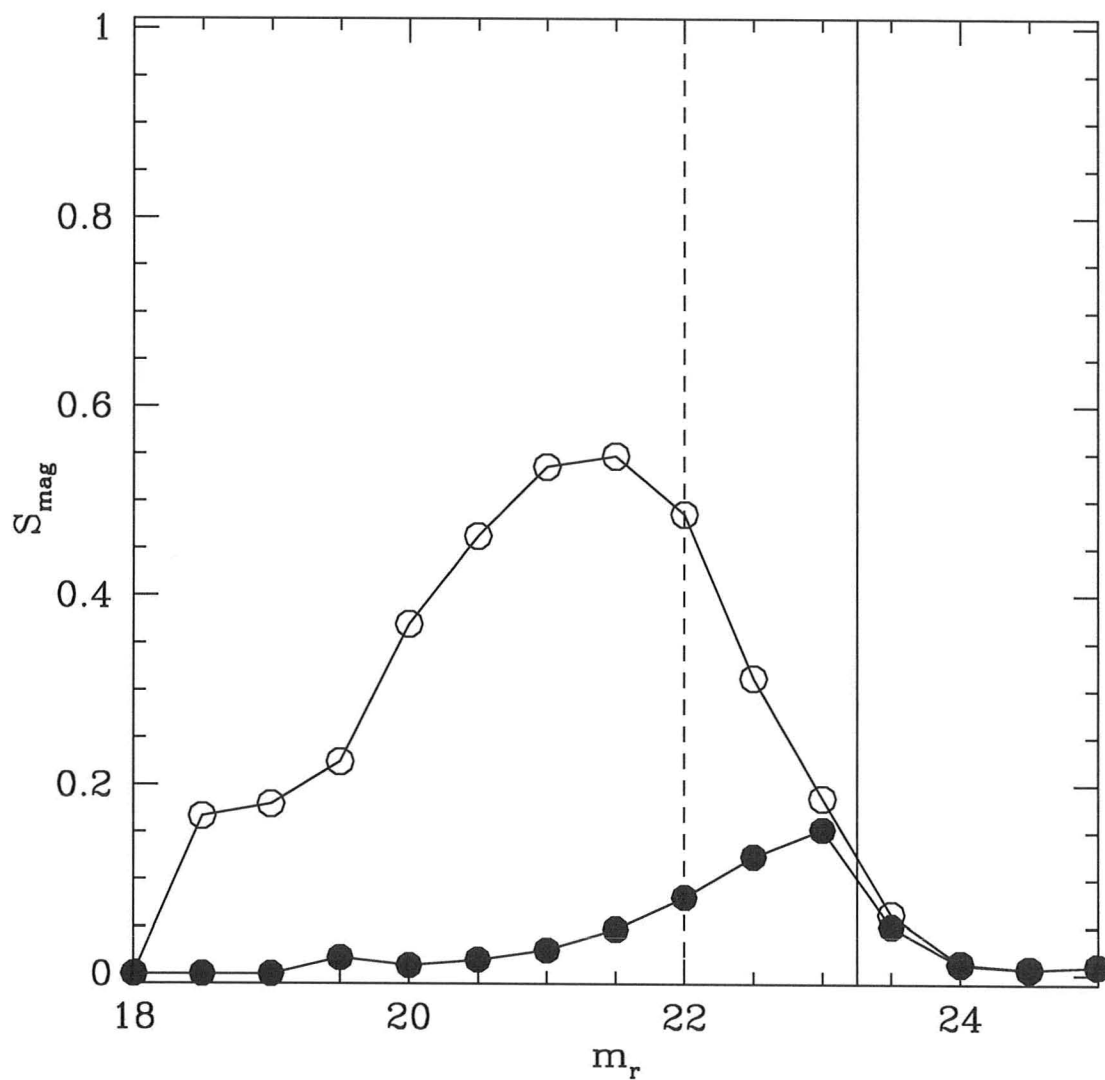


Figure 3.2: The selection functions, S_{mag} , are shown for the total sample (open circles) and the FORS2 sample (filled circles). Our chosen limits for the CNOC2 sample (dashed) and FORS2 sample (solid) are also shown as vertical lines (see next section).

3.3 Luminosities and Colours

3.3.1 Photometric Limits

By combining the information from these weights and the statistical and photometric completeness of our survey, we can define a reasonable magnitude limit beyond which it is implausible to expect that the weights can reasonably account for the deficit in redshift measurements. It is desirable to retain as many of the galaxies as possible, but we also need to keep the sample reasonably robust. The entire completeness weighting scheme depends strongly on our assumption that the survey is photometrically complete down to the spectroscopic limit. We will now investigate this issue.

The full dataset contains photometry from a number of sources. We are most interested in separating galaxies into various evolutionary stages – namely passive and star-forming – and the best photometric age discriminator is $g - r$ colour (or B-R in CFH12k) for the redshift range of our sample. This is because the filters span a region of the spectrum affected by numerous absorption lines blueward of $\sim 4000\text{\AA}$. These absorption lines are more prominent if they are generated by cooler stars. Thus, a large discrepancy would exist if the galaxy is predominantly red, so a colour measured from filters spanning this ‘4000 \AA break’ effectively separates red (older) galaxies from blue (younger) (Gorgas et al., 1999). We would like to use the *ugriz* photometry exclusively, but there

are a few galaxies for which we do not have Megacam photometry; in this case we transform CFH12k magnitudes to the Megacam system via

$$g = B + 0.058 - 0.588(B - V), \quad (3.6)$$

$$r = R - 0.07 + 0.261(V - R), \quad (3.7)$$

$$i = I + 0.119 \quad \text{if } (B - V) > 1, \quad (3.8)$$

$$i = I - 0.11 + 0.2(B - V) \quad \text{if } (B - V) \leq 1 \quad (3.9)$$

if there are enough CFH12k filters available. As reported in Balogh et al. (2009), the resulting magnitudes have a typical standard deviation of 0.05 mag in i and 0.08 mag in r and g . There are a small number (~ 5 per cent) of galaxies for which there is insufficient photometry for analysis, and these are generally objects lying at the edges of our observed fields where imaging is incomplete. Such objects are simply culled from our sample.

It is necessary to remove from our sample galaxies that may have erroneous data. For instance, magnitude errors become a concern at the faintest limits. To explore this issue in our sample, we plot the observed $(g - r)$ colours of galaxies within our FORS2 target areas versus their apparent r magnitude in Fig. 3.3. The large scatter in colour at magnitudes beyond $r = 23$ indicates unreliable photometry. Considering that more than one-third of our redshift sample lies in the magnitude range of $22.75 < r < 23.25$, we choose a photometric limit in the r -band of $r = 23.25$.

We must also be cautious that colours (e.g., $(g - r)$) measured at our r -band magnitude limit will be robust, and this requires that the g -band photometry

be complete down to our limit for the colour range of interest. In Fig. 3.4 we show the number counts of all objects in our photometric sample across the entire region of our 14hr and 21hr patches. The photometric completeness will be better estimated from a larger sample such as this. Shown in the figure are several filters to illustrate the various completeness limits. Photometric data become incomplete beyond the turnover point, where objects become lost due to the detection limit of the observations. Clearly, at our chosen limit of $r = 23.25$, the r -band photometry is complete and unbiased. For the reddest colours ($g - r \sim 2$) the g -band becomes photometrically incomplete. However, the B and V Megacam filters are just barely at the limit, and should provide enough coverage to allow a transformation of CFH12K B band to Megacam g as discussed above. This will help to mitigate the photometric incompleteness, so that our colours are not biased towards blue objects at the faintest magnitudes. Without the B -band coverage we would have to apply brighter cuts and thus lose many of our faintest objects. Galaxies lacking sufficient photometry for our analysis constitute approximately 10 per cent of the sample.

3.3.2 K-corrections

When light emitted from a distant galaxy reaches a telescope on Earth, the spectrum enters our chosen filters having been redshifted. If we wish to measure a band covering a red region of the spectrum, if the galaxy is distant enough, it will actually be a bluer region of the emitted spectrum that we measure. For example, light detected in the r band from a galaxy at $z = 0$

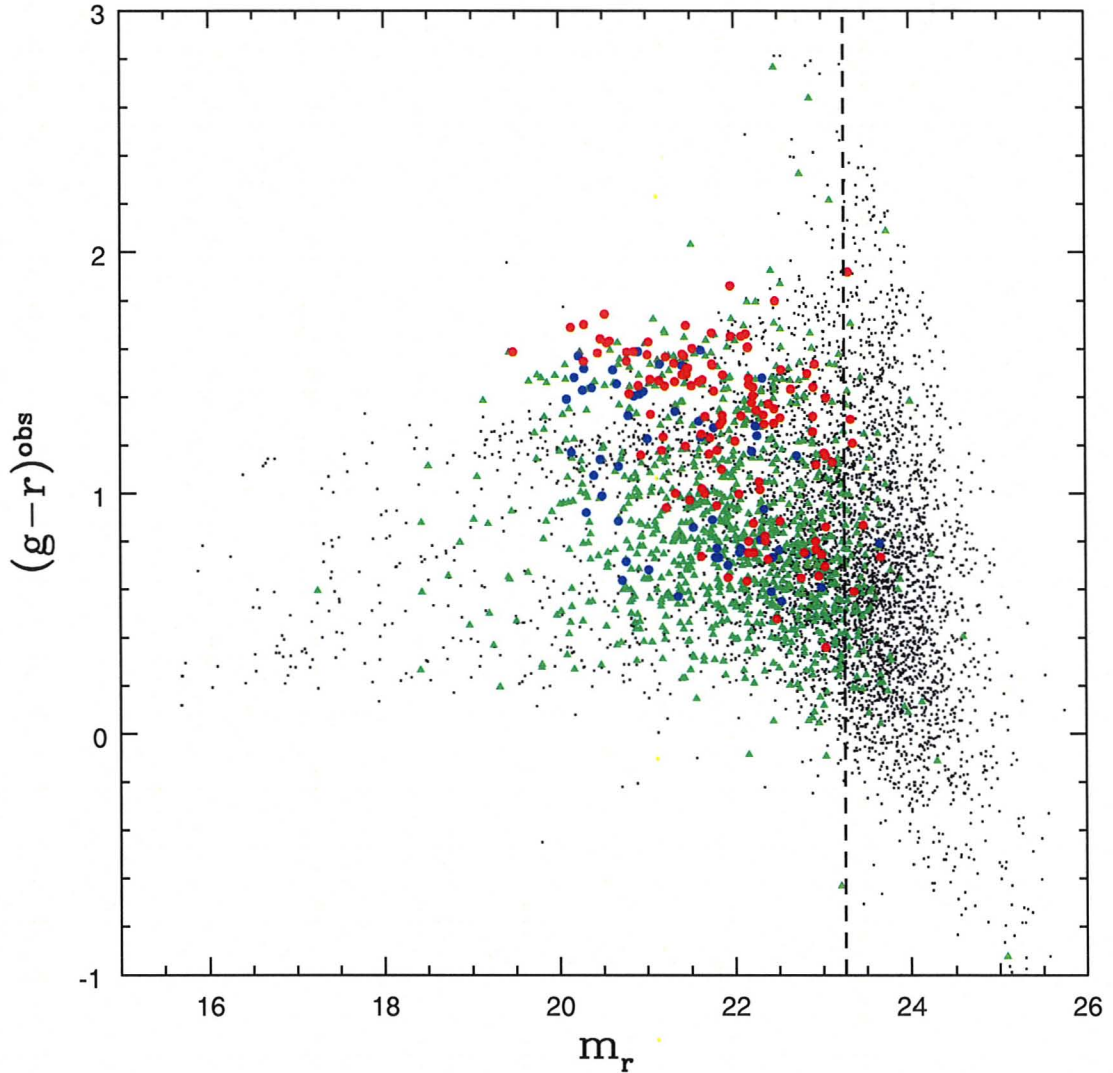


Figure 3.3: Observed $(g - r)$ colours versus apparent r magnitude. Green triangles are galaxies with redshifts, while the circles are group members (splitted into two bins of redshift, red for $z > 0.4$ and blue for $z < 0.4$). Based upon this figure, we can see that the errors in the r magnitudes become large shortly beyond $r = 23$. Our chosen magnitude limit is shown by the vertical dashed line.

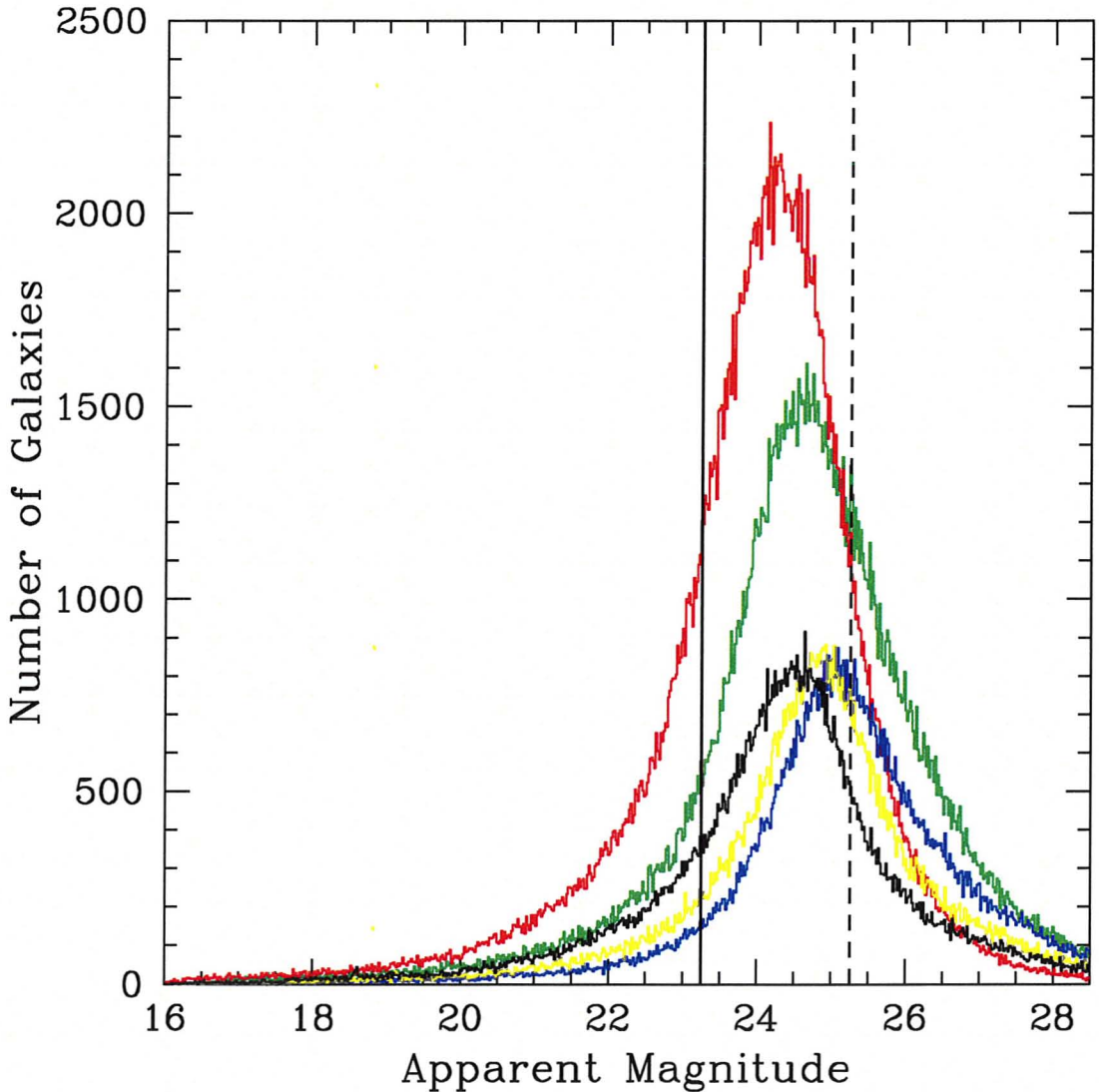


Figure 3.4: Total number counts of galaxies in the entire regions of the two CNOC2 patches (14hr and 21hr) as a function of apparent magnitude for a selection of wavebands, as follows: Megacam r and g are red and green, respectively; CFH12K R , B and v are black, blue and yellow, respectively. The dotted line represents a g band cutoff for $(g-r) = 2$ at our chosen r -band limit (solid line). Photometric completeness becomes poor just after turnover.

(rest-frame) does not sample the same region of the galaxy's spectral energy distribution (SED) if that same galaxy were to be observed at $z = 0.4$ (where the light is redshifted). This alters our photometric measurements (including colours) and it is, therefore, necessary to compensate for this effect. This correction for band-shifting is called a k-correction. The correction depends on the galaxy's SED, and in general we need many filters (as well as the redshift) to calculate it (Oke & Sandage, 1968; Blanton & Roweis, 2007).

Our k-corrections were performed in the same way as described in Balogh et al. (2009), but here we provide a brief summary. For all galaxies with measured redshifts we recompute the k-corrections to include the new FORS2 data using the program `KCORRECT` v4.1.4 (Blanton & Roweis, 2007). Any photometric data that exist (be it Megacam *ugriz* or CFH12K *BVRI*), is used in the native filters for our analysis. However, corrections are only made for galaxies with coverage in at least 4 different filters. Galactic extinction was accounted for with maps from Schlegel et al. (1998), using an average value for our two patches:

$$A_\lambda = -1.415 - 1.5 \log_{10} \lambda / \mu\text{m}. \quad (3.10)$$

For all galaxies, we k-correct to the average redshift of our sample, $z = 0.4$, both to have the magnitudes represent observations at $z = 0.4$ (with no correction for evolution) and so that the size of the k-correction and associated uncertainty are minimised. Fig. 3.5 shows the $(g - r)$ colours of our sample of galaxies before and after k-corrections were applied.

Throughout this paper, we indicate k-corrected absolute magnitudes and colours with the notation $^{0.4}M_X$ and $^{0.4}(X - Y)$, for filter X magnitude and $X - Y$ colours. The superscript indicates the redshift to which the given quantity is k-corrected ($z = 0.4$ in this case).

3.3.3 Colours

In order to distinguish between red and blue galaxies, which is to become important later (see §3.5), we must define the red sequence. Fig. 3.6 shows a colour-magnitude diagram of $^{0.4}(g - r)$ colour versus $^{0.4}M_r$, where the galaxies are bimodally distributed. Bluer galaxies are spread across a region below a fairly tight red sequence of galaxies, divided by a small number of galaxies that is sometimes referred to as the ‘green valley’.

To define our sample of red galaxies, we examine the colour distribution in Fig. 3.7, and observe the bimodal distribution of galaxies. Also plotted is the distribution split into our group and field samples. We choose first a cut of $^{0.4}(g - r) > 1.15$, and use those galaxies in a least-squares fitting routine to fit the red sequence. We then subtract 0.15 mag from this fit to define our sample of ‘red sequence galaxies’. This offset from the red sequence represents approximately one standard deviation in the scatter of red galaxies from the fitted line. The red sequence is highlighted in Fig. 3.6 as the red line. Group members are shown as the filled circles, while the remainder of the sample is represented by points.

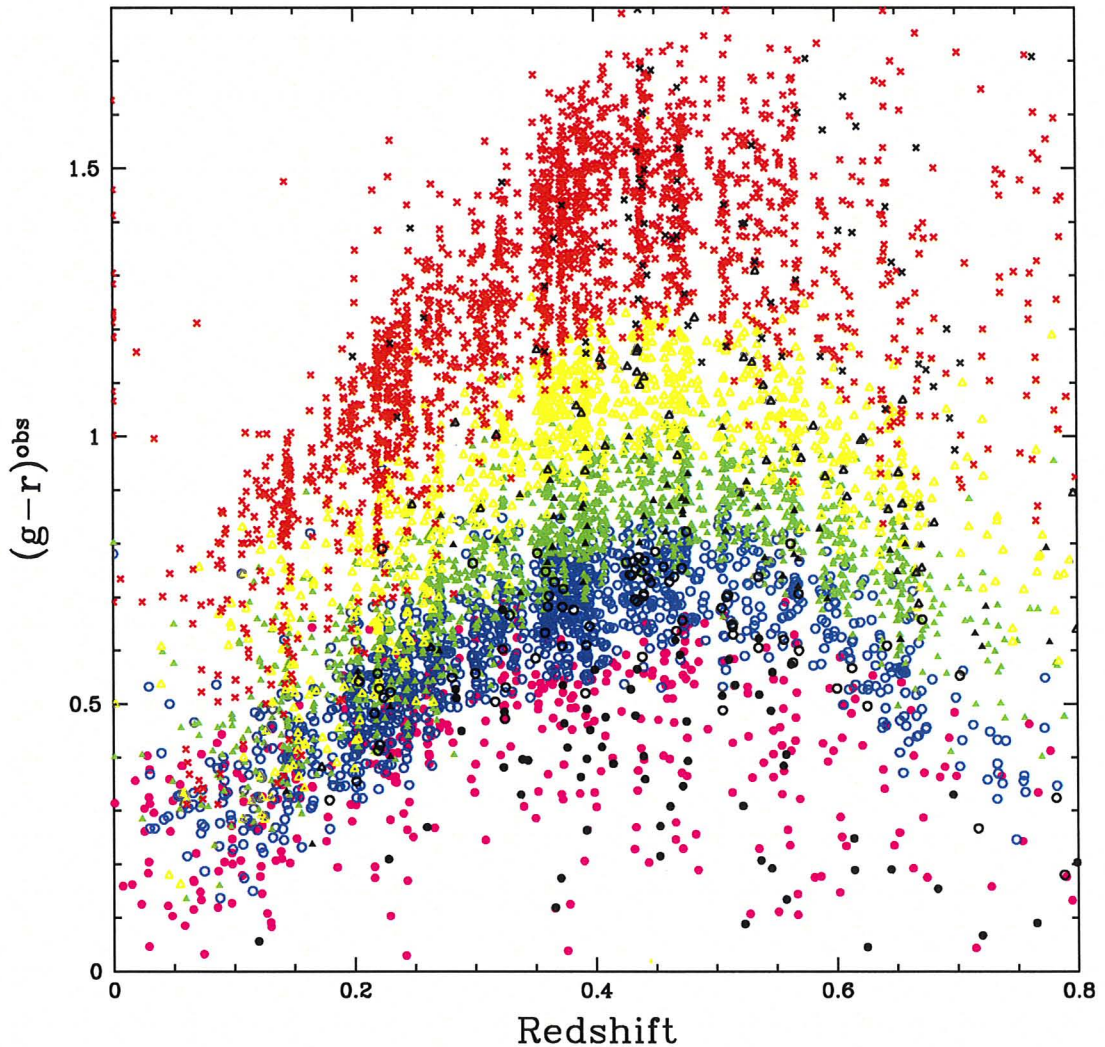


Figure 3.5: Observed $(g-r)$ colours of galaxies plotted against redshift, colour-coded according to their k-corrected colours. This figure is drawn from Balogh et al. (2009), but with the addition of the FORS2 data, shown all in black symbols. The symbol types are also coded according to their k-corrected colours. The magenta filled circles are galaxies with $^{0.4}(g-r) < 0.6$, and the remaining blue (open circles), green (filled triangles), yellow (open triangles) and red (crosses) represent, respectively, successive bins of colour 0.2 magnitudes wide (with the final bin's colour $^{0.4}(g-r) > 1.2$). The consistent segregation of colours indicates that the k-corrections are robust.

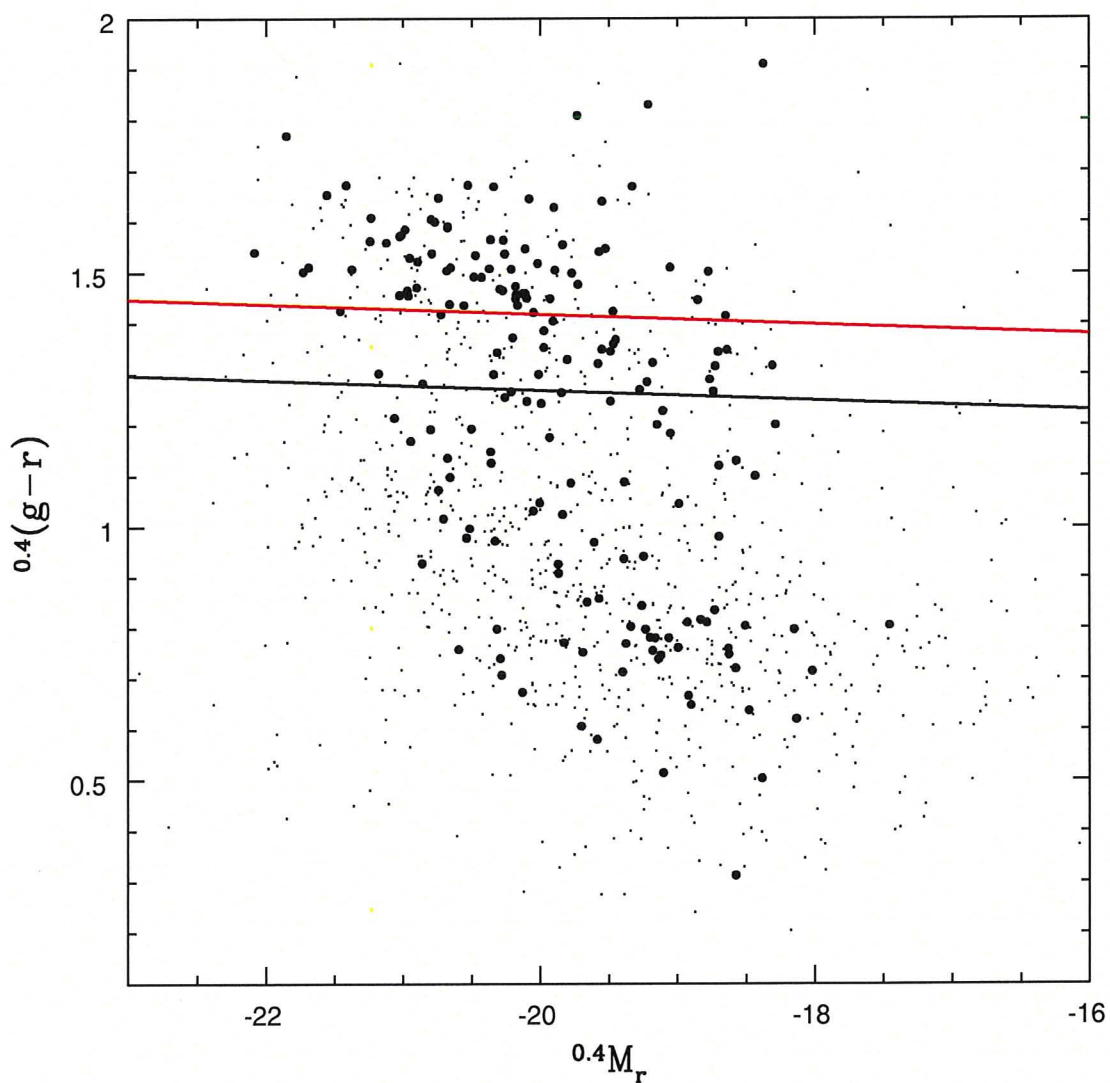


Figure 3.6: The $0.4(g-r)$ colours of galaxies plotted against $0.4M_r$ ($3''$ aperture). The black solid line, which is 0.15 mag below a fit to the red sequence (red solid line), is our chosen cut separating the 'red' and 'blue' galaxies. Dots indicate the field sample, while filled circles are group members.

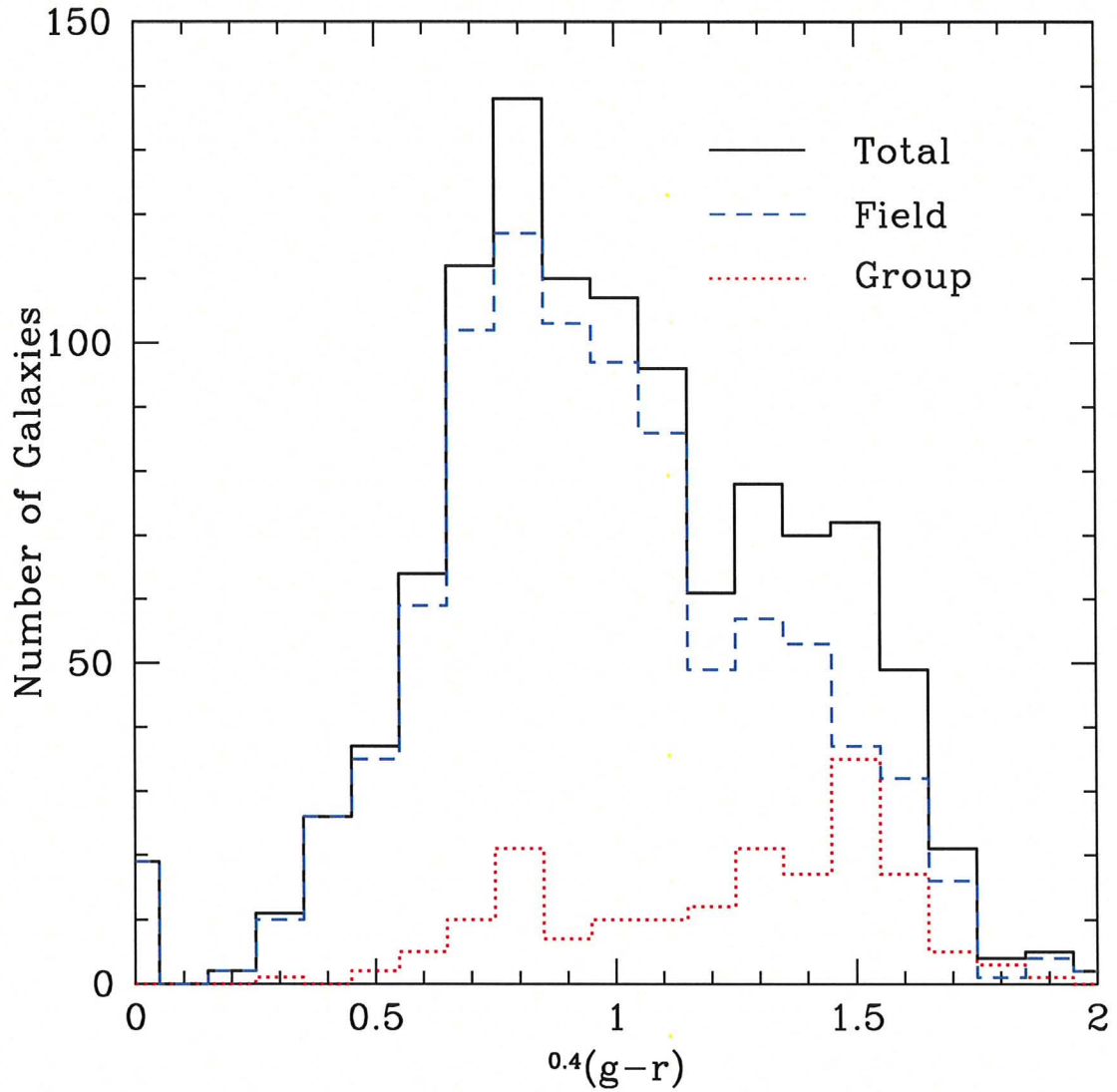


Figure 3.7: The distribution of $^{0.4}(g-r)$ colours of our sample. We show the total sample with the solid line, along with the group and field samples (as defined in the text) as the dotted and dashed lines, respectively.

3.4 Luminosity Functions

One of the fundamental ways in which we can characterise a population of galaxies is simply counting them, organised by some other basic parameter such as luminosity or stellar mass. In particular, the galaxy luminosity function (LF) shows us the relative contributions of the galaxies of various magnitudes (or luminosities) to the total population. A number of physical mechanisms play a role in shaping the LF (e.g., Rees & Ostriker, 1977; White & Rees, 1978; Benson et al., 2003), and comparing results from different populations is useful when studying galaxy evolution (e.g., Lin et al., 2004; Balogh et al., 2007).

Individually, groups contain an insufficient number of member galaxies to compute a statistically robust LF. Therefore, we stack our groups together and construct a composite LF. This will represent an average group from our sample.

A common way to quantify luminosity functions is to fit them with the Schechter function (Schechter, 1976):

$$\Phi(L)dL = \Phi^* \left(\frac{L}{L^*} \right)^\alpha e^{-L/L^*} d \left(\frac{L}{L^*} \right), \quad (3.11)$$

in which $\Phi(L)dL$ is the number of galaxies between L and $L + dL$, Φ^* is an overall normalisation, L^* is a characteristic luminosity, and α is the faint end

slope. Typically, depending on the environment, α is on the order of -1 . In terms of absolute magnitude, this function can be transformed into the form

$$\Phi(M)dM = \frac{2}{5} \ln(10) \Phi^* 10^{\frac{2}{5}(\alpha+1)(M^*-M)} e^{-10^{0.4}(M^*-M)} dM. \quad (3.12)$$

In this case, we have a characteristic absolute magnitude, M^* , instead of a characteristic luminosity.

To compute our luminosity function, we separate the galaxies into one-magnitude bins of absolute k-corrected r magnitude and count the number of group members in each bin, weighted by completeness correction weights as discussed in §3.2. Each group is at a different redshift, and thus will have a different absolute luminosity limit. To correct for this, we apply a correction weight as follows:

- For each group we compute its absolute magnitude limit to be the faintest galaxy contained within that group. The LF bins beyond this limit are then inaccessible to this group, and the first bin to experience this decrease in contributions from groups defines the LF completeness limit.
- Let's denote the bins brighter than this limit to be 'complete bins', and bins fainter than this completeness limit to be 'incomplete bins'. These are bins that do not have every group contributing to its value.
- Complete bins receive a weight of 1 in the LF.
- For each incomplete bin, we compute the weight to be the ratio of *the sum of all (weighted) galaxies of all groups in all complete bins* to the

sum of all (weighted) galaxies' contributions to complete bins from groups that access the incomplete bin. As an example, suppose that we have a LF consisting of 3 bins of magnitude (bright, intermediate, and faint), composed of 3 groups (g1,g2,g3) of weighted numbers of galaxies in each bin as follows. bright (1,2,3), intermediate (-,4,5), and faint (-,-,6). The totals for each bin are, respectively, 6, 9, 6. The intermediate bin is the first incomplete bin. We thus weight the intermediate bin by the quantity $(1 + 2 + 3)/(2 + 3)$. For the faint bin, the weight is then $(1 + 2 + 3)/3$.

- Finally, each bin is divided by 10, the number of groups in our sample. The result is then the number of galaxies *per group, per magnitude bin*.

Note that this requires an assumption that each group has the same LF, so our result is an average across all of our groups.

For the field LF, we compute the number of galaxies in each magnitude bin for galaxies not belonging to one of our groups but within a redshift range defined by the lowest and highest redshift groups in our sample (see Table 2.1). We employ the V_{\max} method (Felten, 1977) to compute the field LF, which gives each galaxy a volume correction weight equal to the ratio of the cosmological volume over our sample's redshift range ($z_{\text{low}} < z < z_{\text{high}}$) to the 'visible' cosmological volume of the galaxy (V_{\max}). The value of V_{\max} is computed by determining the redshift where we would have found the galaxy if it had been at our apparent magnitude limit, z_{lim} . Then, V_{\max} is the difference between the volume of the lower limit of our sample, z_{low} , and z_{lim} .

Our luminosity functions are plotted in Fig. 3.8. A least squares routine is used to fit a Schechter function form to the group LF, giving $(\phi^*, M^*, \alpha) =$

$(24 \pm 9, -20.7 \pm 0.3, -1.0 \pm 0.3)$. We are interested in comparing M^* and α between our group and field samples, so the overall normalisation is less important. Thus, for display purposes, we normalise the field luminosity function to the total number of (weighted) galaxies in our average group LF. The field LF is difficult to fit with a Schechter function, as its shape is very different from the group LF. Therefore, we choose to fix the value of Φ^* to the group value of 24 (since we normalised it that way), and fit the remaining parameters. The result is $M^* = -19.79 \pm 0.04$ and $\alpha = -1.35 \pm 0.09$. While the shape of the field LF hints that there are proportionately more faint galaxies and fewer bright galaxies in the field than in our groups, it must be kept in mind that the uncertainties on the faint end slope are large and the group and field are statistically indistinguishable. Additionally, the Schechter form is not an ideal shape for our LFs, as indicated by a large χ^2 value. Thus, it is very difficult to constrain despite our faint data.

3.4.1 A Comparison Between Red and Blue Galaxies

A way of showing the red fraction of galaxies (other than red fractions, as we will see in §3.5) is to disentangle the red and blue galaxies that compose the LF in the preceding subsection. That is, we can plot the LF as two histograms (one each for red and blue galaxies) which sum to the original group LF. We show such a plot in Fig. 3.9, which demonstrates the relative contributions of red and blue galaxies to the group environment in bins of absolute magnitude. It is clear from this analysis that red galaxies dominate the group environment

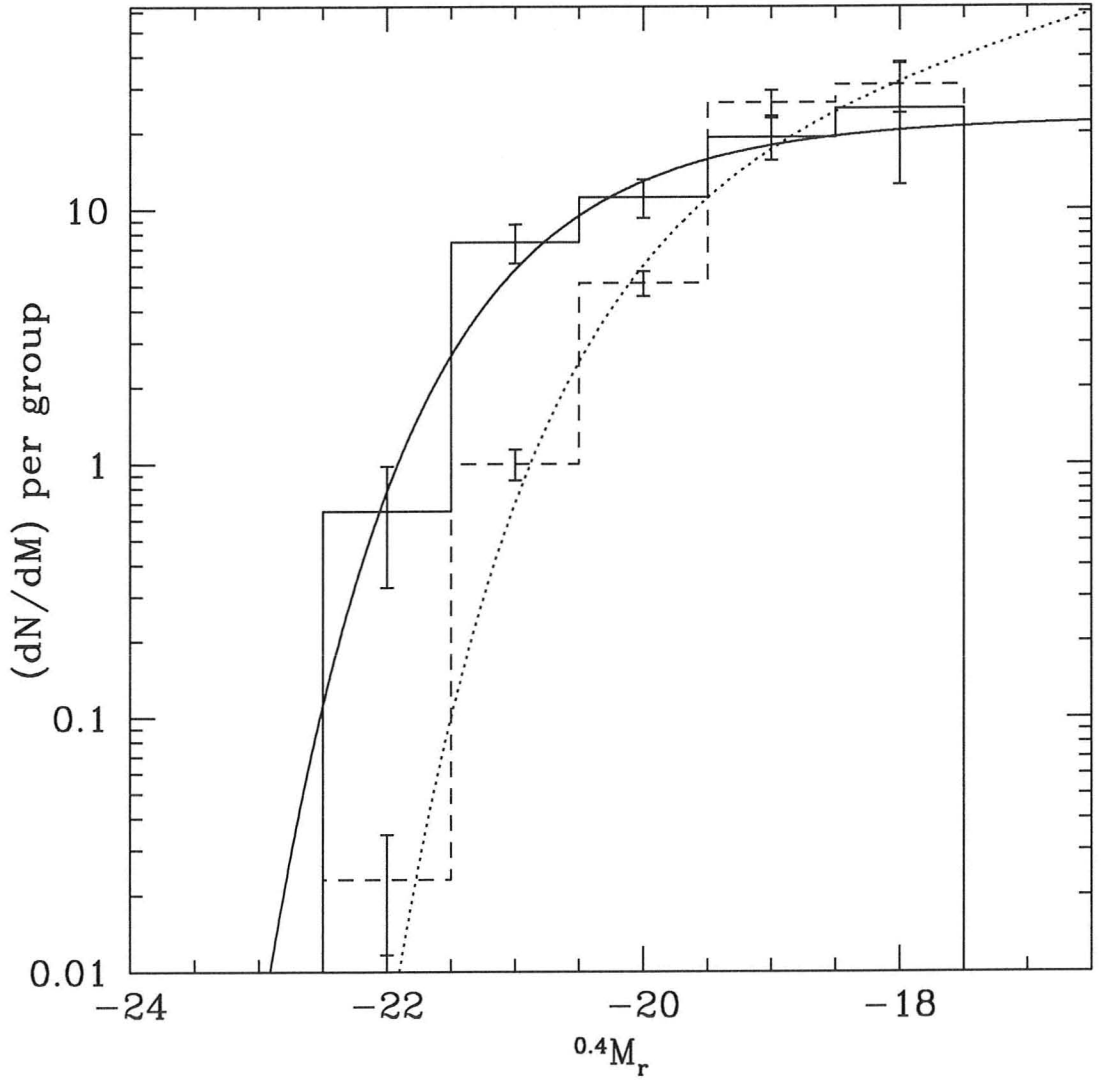


Figure 3.8: LF comparing groups to the field environment in our sample. The solid histogram is the stacked group, and the solid line a Schechter function fit to the data. The dotted histogram and fit is the field. Error bars are computed assuming Poisson statistics.

at magnitudes brighter than $^{0.4}M_r = -20$, with blue galaxies being the major component at the faint end.

3.4.2 Trends in Group Mass

By separating the low and high velocity dispersion groups and computing their individual LFs, we can ascertain any differences in their respective galaxy populations. The four groups with velocity dispersion larger than 400 km s^{-1} in Table 2.1 define our high- σ sample, and the six remaining groups define our low- σ sample. We prefer not to divide evenly into five groups each since two groups have velocity dispersions very close to the median, and the higher mass groups have many more members, which helps to even out the statistical uncertainties. Our LFs are shown in Fig. 3.10, where the solid histogram is the high- σ sample and the dashed histogram is the low- σ sample. Again, the solid curve is the Schechter function fit to the original composite group LF. We find no significant difference between the two group samples, except that the faintest galaxies are found only in the low- σ sample. Future work will involve computing the stellar mass function (the number of group galaxies per group per bin of stellar mass), which will allow a direct comparison of the stellar mass in the two velocity dispersion samples.

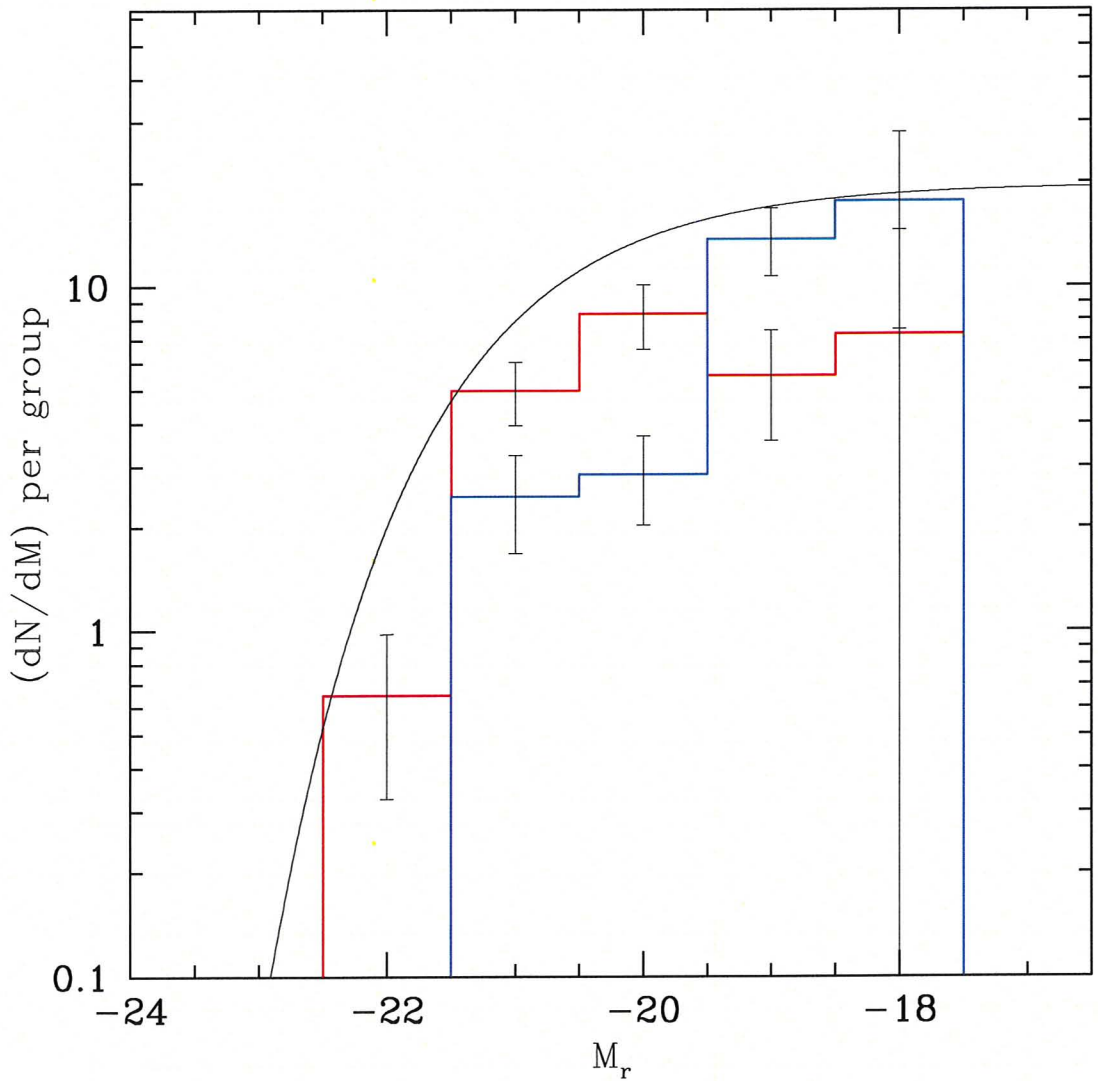


Figure 3.9: Splitting the group LF into red and blue components reveals a trend of red galaxies dominating the group environment at brighter magnitudes. The histograms, colour-coded as red or blue, are computed in such a way that their sum returns the original group LF. Error bars are computed assuming Poisson statistics.

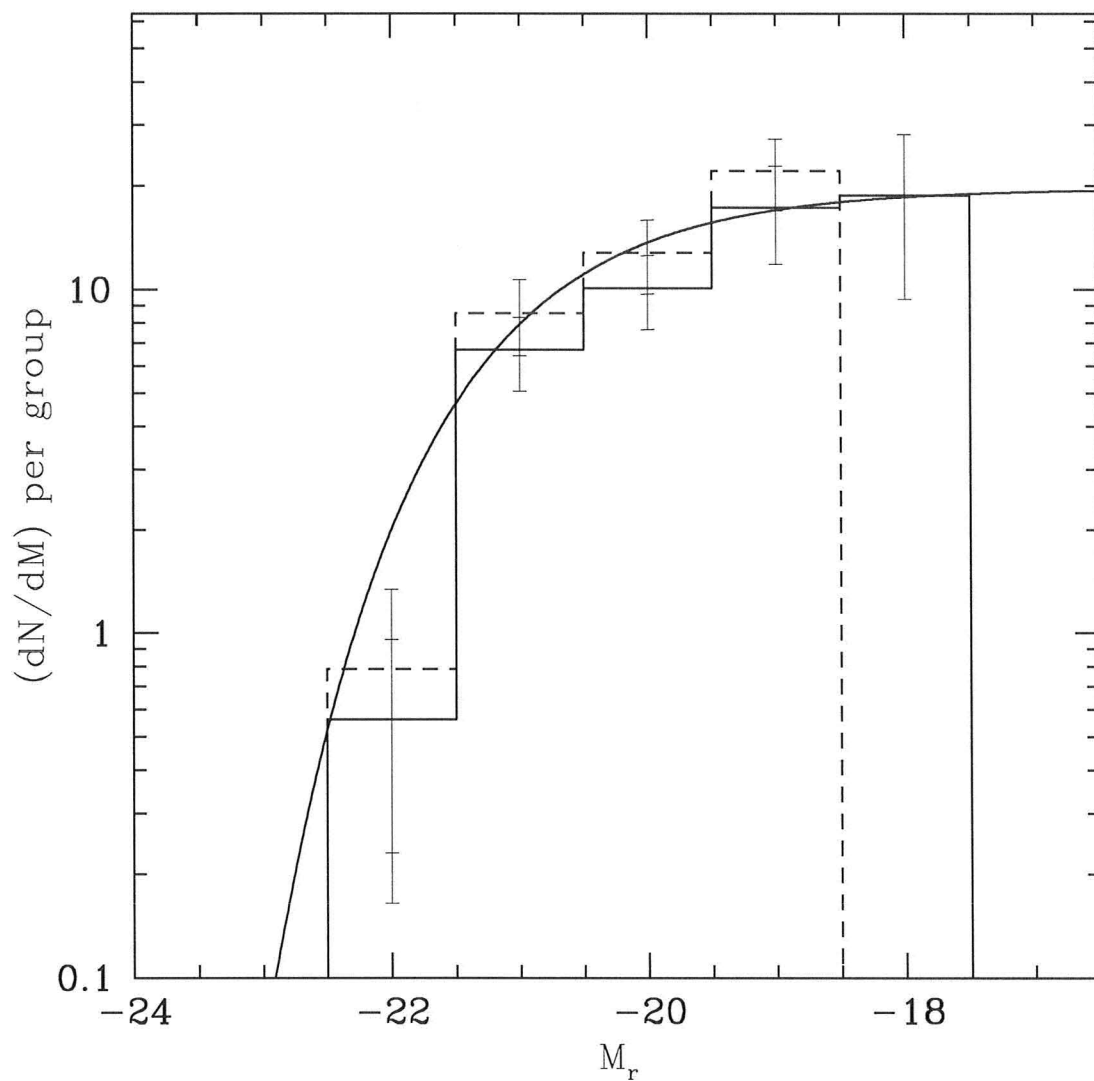


Figure 3.10: Comparing the LF for low and high velocity dispersion groups. The low- σ groups are shown as the solid histogram LF, while the high- σ group LF is the dashed histogram. The solid line is our fit to the composite group.

3.5 Red Fractions

We now compute the relative contribution of red and blue galaxies in our sample of galaxy group members. We take the red sequence galaxies to be those lying above the black line in Fig. 3.6. We separate our galaxies into absolute magnitude bins of 1 mag width, and compute the ratio of the number of red galaxies to the total number of galaxies in each bin, where each galaxy is weighted to correct for completeness as described in §3.2.

The results are shown in Fig. 3.11, in which the filled points are group members, and the circles are field galaxies. Error bars are computed using binomial statistics (Gehrels, 1986). At all magnitudes brighter than $^{0.4}M_r = -18$, the group environment contains a higher fraction of red galaxies compared to the field. In fact, all galaxies in our group sample are red at the brightest magnitudes. While both the field and group red fractions decline toward the faint end, it appears that, at the faintest magnitudes, group and field galaxies have similar colours (that is, blue).

To understand variations within the group sample, we also compute the total red fraction of galaxies in groups separated into two bins of velocity dispersion. We find that the red fraction of the high- σ groups is $0.42_{-0.07}^{+0.07}$. However, the red fraction of the low- σ groups is significantly higher, $0.61_{-0.08}^{+0.07}$.

Overall, the group red fraction is $0.51_{-0.05}^{+0.05}$, while the field is $0.17_{-0.02}^{+0.02}$. This is not surprising, given the well-known trend for red galaxies to be found preferentially in high density environments (e.g., De Lucia et al., 2004; Balogh et al., 2009).

Table 3.1: Red fractions for a variety of sample cuts, as shown. The rows are divided into samples of all, bright, and faint galaxies as defined in the text. All columns refer to group galaxies, except for the field. The samples are defined as: $-22.5 < {}^{0.4}M_r < -17.5$ (all); $-22.5 < {}^{0.4}M_r \leq -19.5$ (bright); and $-19.5 < {}^{0.4}M_r < -17.5$ (faint).

| All Groups | High- σ | Low- σ | $r \leq R_{200}$ | $r > R_{200}$ | Field |
|------------------------|------------------------|------------------------|------------------------|-----------------------|------------------------|
| All Galaxies | | | | | |
| $0.51^{+0.05}_{-0.05}$ | $0.42^{+0.07}_{-0.07}$ | $0.61^{+0.07}_{-0.07}$ | $0.52^{+0.06}_{-0.07}$ | $0.49^{+0.09}_{-0.1}$ | $0.17^{+0.02}_{-0.02}$ |
| Bright Galaxies | | | | | |
| $0.74^{+0.06}_{-0.08}$ | $0.55^{+0.09}_{-0.10}$ | $0.91^{+0.07}_{-0.12}$ | $0.64^{+0.08}_{-0.10}$ | $0.8^{+0.1}_{-0.2}$ | $0.26^{+0.03}_{-0.03}$ |
| Faint Galaxies | | | | | |
| $0.3^{+0.1}_{-0.1}$ | $0.3^{+0.2}_{-0.1}$ | $0.3^{+0.2}_{-0.1}$ | $0.45^{+0.15}_{-0.14}$ | $0.0^{+0.3}_{-0.0}$ | $0.09^{+0.04}_{-0.03}$ |

We can also examine the fainter galaxies by splitting our sample in two to form ‘bright’ and ‘faint’ samples defined by an absolute magnitude cut of ${}^{0.4}M_r = -19.5$. We find that the red fractions for the low- and high- σ groups become statistically indistinguishable at the faint end, at $\sim 0.3^{+0.2}_{-0.1}$. A clear difference arises at the bright end, where a large fraction ($0.91^{+0.07}_{-0.12}$) of the low- σ group galaxies are red. These results are summarised in Table 3.1. In that table we also include red fractions of our sample cut into bins of radial distance from the group centroid, which will be discussed in §4.1

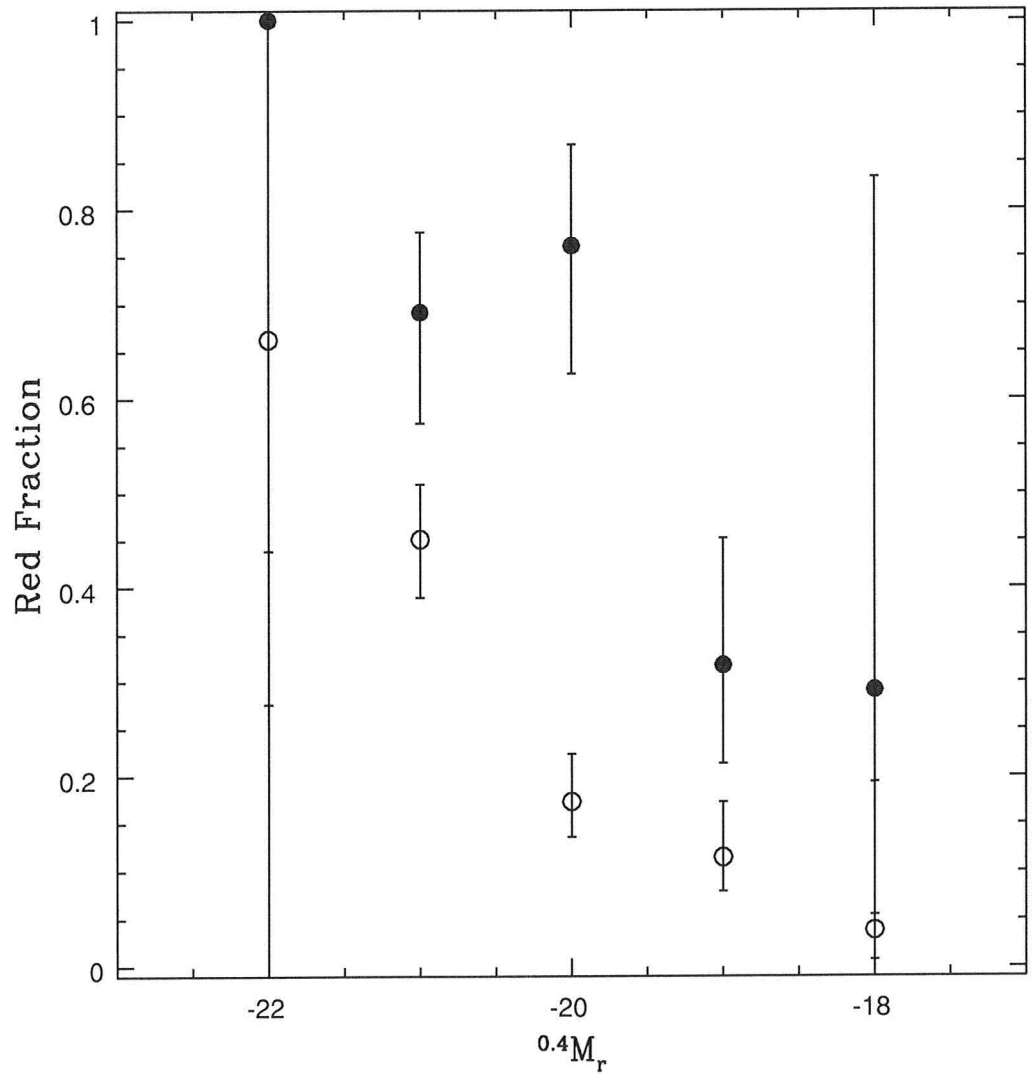


Figure 3.11: Red fractions for the group (filled symbols) and field (circles) galaxies, weighted to correct for incompleteness.

Chapter 4

Discussion and Conclusions

In the following chapter, we will discuss some systematic effects in our sample, and present our results in the context of previous studies. To begin, we will explore how our LFs and red fractions change depending on our choice of radial cut, and the effects of our new group members on recent dynamical analyses performed on the GEEC sample. We will then compare our results to similar studies at other redshifts (i.e., evolution). To finish, we will present a summary of this work, implications for future work on the GEEC sample, and end with a few concluding remarks.

4.1 Radial Trends

It is important to put a physically reasonable limit on the projected distance, from the centre of a group, out to which a galaxy is deemed to be a member of that group. As discussed in §3, a fairly common radial cut is R_{200} ; in our groups this corresponds to a few hundred kpc. However, due to the large number of galaxy associations beyond this distance, we have chosen in this work to place the limit at 1 Mpc. In this section we will explore the effects

that this has on our results by comparing basic properties of the galaxies both within R_{200} and between R_{200} and 1 Mpc.

In Fig. 4.1 we show LFs composed of two samples of group galaxies based on their radial positions, as defined above. There is no significant difference in the two samples except in the brightest bin, where the LFs suggest that most of the brightest group galaxies are within R_{200} .

For the red fractions of galaxies within R_{200} and between R_{200} and 1 Mpc, we find no difference overall, as both have red fractions of $\sim 0.5 \pm 0.1$. For the bright galaxies, there is no statistically-significant difference in the two samples. However, while the difference is barely at 1σ , there is an indication that the faint galaxies within R_{200} are redder than those outside of R_{200} ; in fact, we find *no* faint red galaxies outside of R_{200} .

4.2 Dynamical Effects of the Faint Galaxies

Studies on the dynamics and dynamical states of groups and clusters of galaxies are becoming more common as the efficiency of spectroscopic observations increases. Dynamical studies rely on information about the positions and radial velocities of each member galaxy. Thus, it is natural to expect that with more complete redshift information (i.e. more members) uncertainty in dynamical analyses can be reduced.

In the work of Hou et al. (2009), the Anderson-Darling statistical test was employed to classify the galaxy groups in our GEEC sample as either dynamically relaxed (\sim Gaussian) or dynamically complex (non-Gaussian).

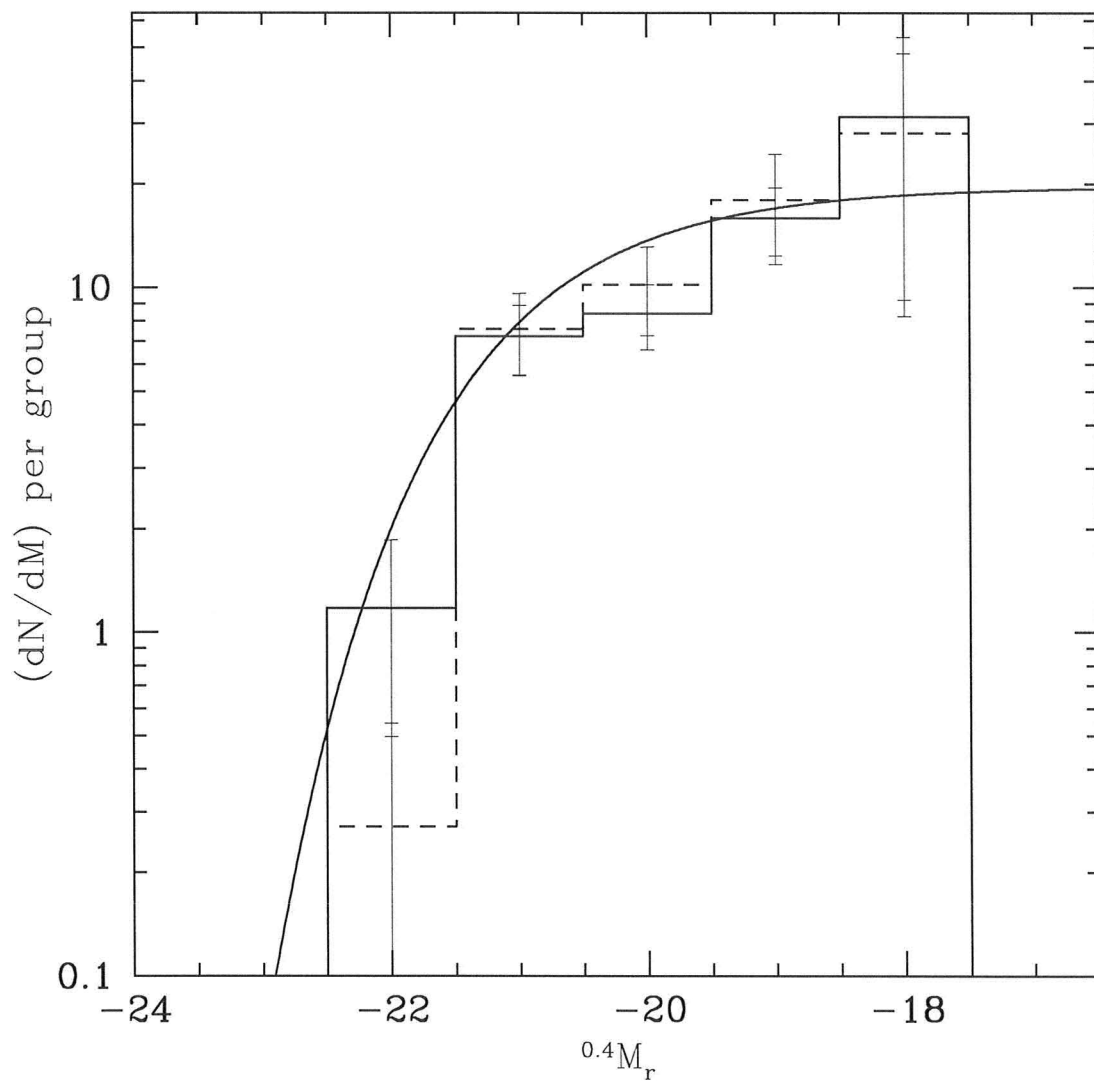


Figure 4.1: Luminosity functions of composite group samples composed of members either within or outside a radial cut of R_{200} , but within 1 Mpc. The dotted line indicates $r < R_{200}$, and the solid line indicates $R_{200} < r < 1$ Mpc.

Approximately 32 percent of all GEEC groups were classified as the latter, four of which are present in our sample of 10 groups (Groups 24, 38, 138, 139). We are now interested to see if the addition of our fainter FORS2 group members alters this classification and their measured velocity dispersions.

Using the techniques outlined in Hou et al. (2009), we show the results of adding the additional group members to the dynamical analysis in Table 2 (analysis performed by Annie Hou). Two of our groups have their classifications change: groups 37 and 39 go from a Gaussian classification to non-Gaussian. In addition, while the velocity dispersions are modified somewhat, the changes are on the order of a few to ~ 15 per cent, which is within the tolerance of the velocity dispersion uncertainties. Thus we find no statistically significant differences in the σ measurements. However, we conclude that adding these few faint members may change dynamical classifications, although this awaits further analysis to determine the effects of group members lying beyond the dynamical radius (R_{200}).

4.3 Evolution

One of the most interesting questions we can address concerns the evolution of faint galaxies as a function of environment. To do this, we will compare our group LF and red fractions to results from similar studies at different redshifts.

Table 4.1: Results of the dynamical state analysis both with and without the new FORS2 data. Shown here, in the columns, are the group IDs, old and new velocity dispersions, and the dynamical classifications (Gaussian/non-Gaussian) both with and without the new FORS2 data.

| Group ID | N_{mem} | $\sigma_{\text{intr}}^{\text{old}}$ ($km\ s^{-1}$) | $\sigma_{\text{intr}}^{\text{new}}$ ($km\ s^{-1}$) | G/NG ^a (prev.) | G/NG ^a (with FORS2) |
|------------|------------------|---|---|------------------------------|-----------------------------------|
| 14hr Field | | | | | |
| 24 | 13 | 42 | 35 | NG | NG |
| 25 | 17 | 470 | 473 | G | G |
| 28 | 7 | 161 | 144 | — ^b | NG |
| 37 | 14 | 236 | 244 | G | NG |
| 38 | 19 | 793 | 754 | NG | NG |
| 39 | 18 | 461 | 442 | G | NG |
| 21hr Field | | | | | |
| 134 | 12 | 315 | 280 | G | G |
| 137 | 10 | 314 | 304 | G | G |
| 138 | 38 | 731 | 776 | NG | NG |
| 139 | 13 | 226 | 200 | NG | NG |

^a A Gaussian classification requires $\alpha < 0.05$ in the A-D test, as defined in Hou et al. (2009).

^b Group 28 had too few members for the test without the new FORS2 data.

4.3.1 Low-redshift Luminosity Functions

Our LF comparison will be with the low- z work of Miles et al. (2004), which consists of a study of a sample of groups going out to distances no greater than $z = 0.016$ (~ 70 Mpc). Twenty-five groups were selected from the Group Evolution Multiwavelength Study (GEMS)¹ for this study, some of which also have detections in the X-ray (Osmond & Ponman, 2004). Group galaxies were selected as being probable members by means of background subtraction and colour. Specifically, they make a cut in colour by first selecting all galaxies with $(B - R) < 1.7$ to exclude the majority of high-redshift background objects.² Their background subtraction then depends on the LF of galaxies outside of R_{500} . The remaining galaxies were then taken to be group members.

Miles et al. (2004) present LFs in the R -band of these groups, split into two categories based upon their X-ray luminosities. The threshold dividing the samples is $L_X = 10^{41.7}$ erg s^{-1} . This corresponds to approximately 300 km s^{-1} , near the division of our two samples of high- σ and low- σ groups, according to a standard $L_X - \sigma$ relation (see Fig. 8 in Finoguenov et al. (2009)). We recompute our LFs in exactly the same way as before, but using magnitudes in the R -band, with bins corresponding to the Miles et al. (2004) LFs. In cases where there is no R -band coverage, we transform from r using the conversions in Balogh et al. (2009). The results are shown in Figs. 4.2 and 4.3. Our LFs were normalised so that they match the Miles et al. (2004) best-fit Schechter

¹ <http://astronomy.swin.edu.au/gems/>.

² Fukugita et al. (1995) showed that all elliptical galaxies with colour $(B - R) > 1.7$ were at $z > 0.2$.

function value of $M^* = -20.1$ for the X-ray-bright groups, and $M^* = -20.5$ for the X-ray-dim groups.

In both of the samples, the LFs hint at a slight excess of fainter galaxies and fewer bright galaxies in our high- z groups relative to the GEMS low- z groups. While we must be mindful of the different targetting strategies and group-finding algorithms, this may be an indication that fainter galaxies were still significant contributors to the group LF, at least since $z \sim 0.4$. This effect also appears to be more apparent in the low- σ groups. Our ability to understand the LF at $z > 0$ is clearly limited by our access to fainter galaxies; this is well evidenced by the significant sample of GEMS galaxies that are much fainter than our own.

4.3.2 Evolution in Group Galaxy Colours

We now show how our red fractions fit in with similar studies on galaxy groups at various redshifts. This will allow us to examine the evolution of the group galaxy red sequence. For groups with membership comparable to this study ($N \sim 20$), Hansen et al. (2009) find red fractions of galaxies to be $f_{\text{red}} = 0.81 \pm 0.01$ for a $0.1 < z < 0.25$ sample, and $f_{\text{red}} = 0.76 \pm 0.01$ for a $0.25 < z < 0.3$ sample, indicating an increased population of red galaxies in groups with time. Their results are consistent with our result that the total red fraction for our $z \sim 0.4$ sample is $f_{\text{red}} \sim 0.5$. Also relevant are the results of Gerke et al. (2007), who indicate that at $z \sim 0.75$ the overall red fraction is $f_{\text{red}} \sim 0.5$. Our results would indicate that the group red fraction is relatively stable over the time period $0.4 \lesssim z \lesssim 0.75$, then increasing toward lower z .

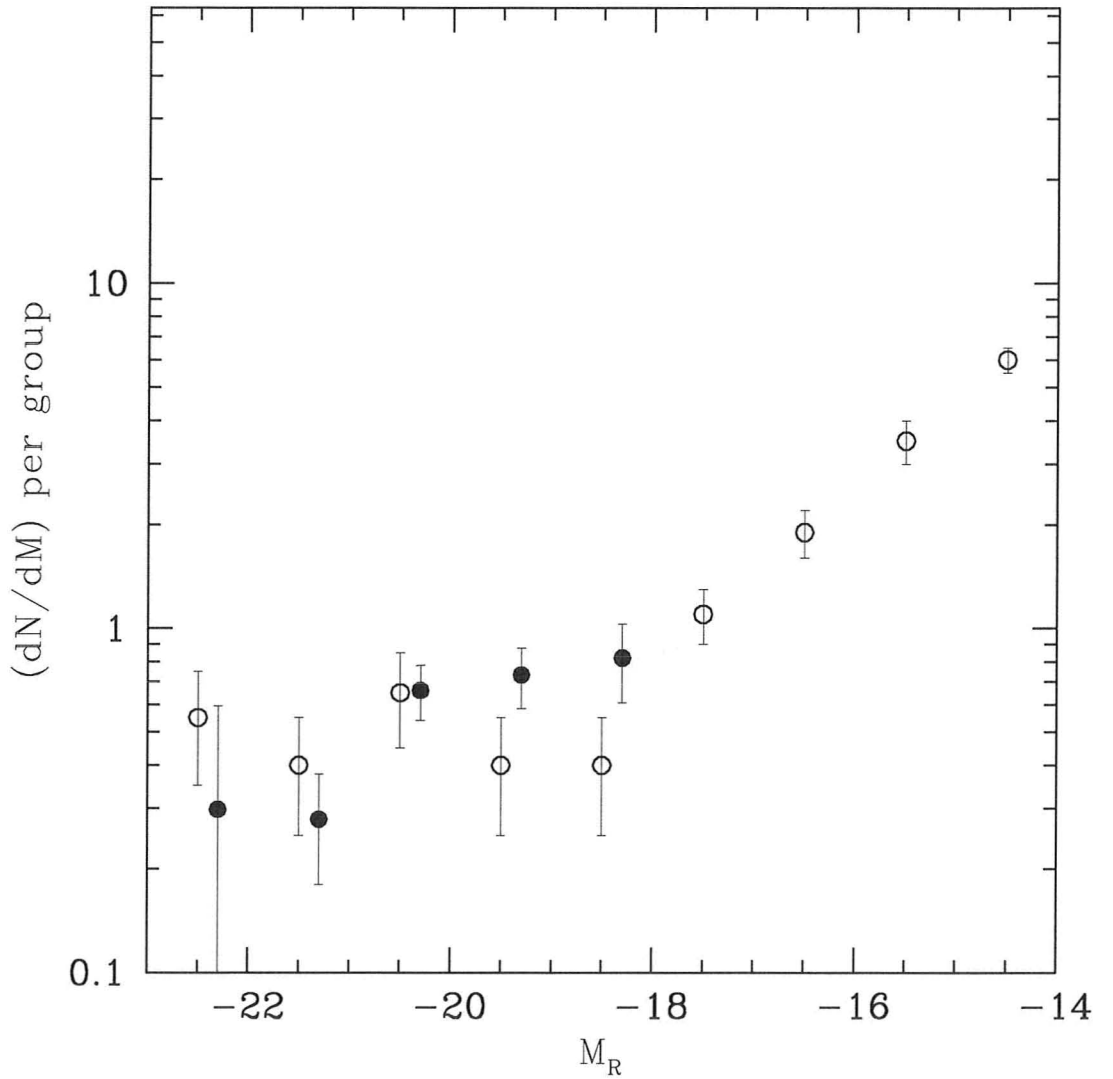


Figure 4.2: Low- σ (or L_X) group LFs from the GEMS sample (empty circles) and this work (filled circles). Our LF was normalised to match the GEMS LF at their M^* . Data points from this work are offset slightly in M_R for clarity.

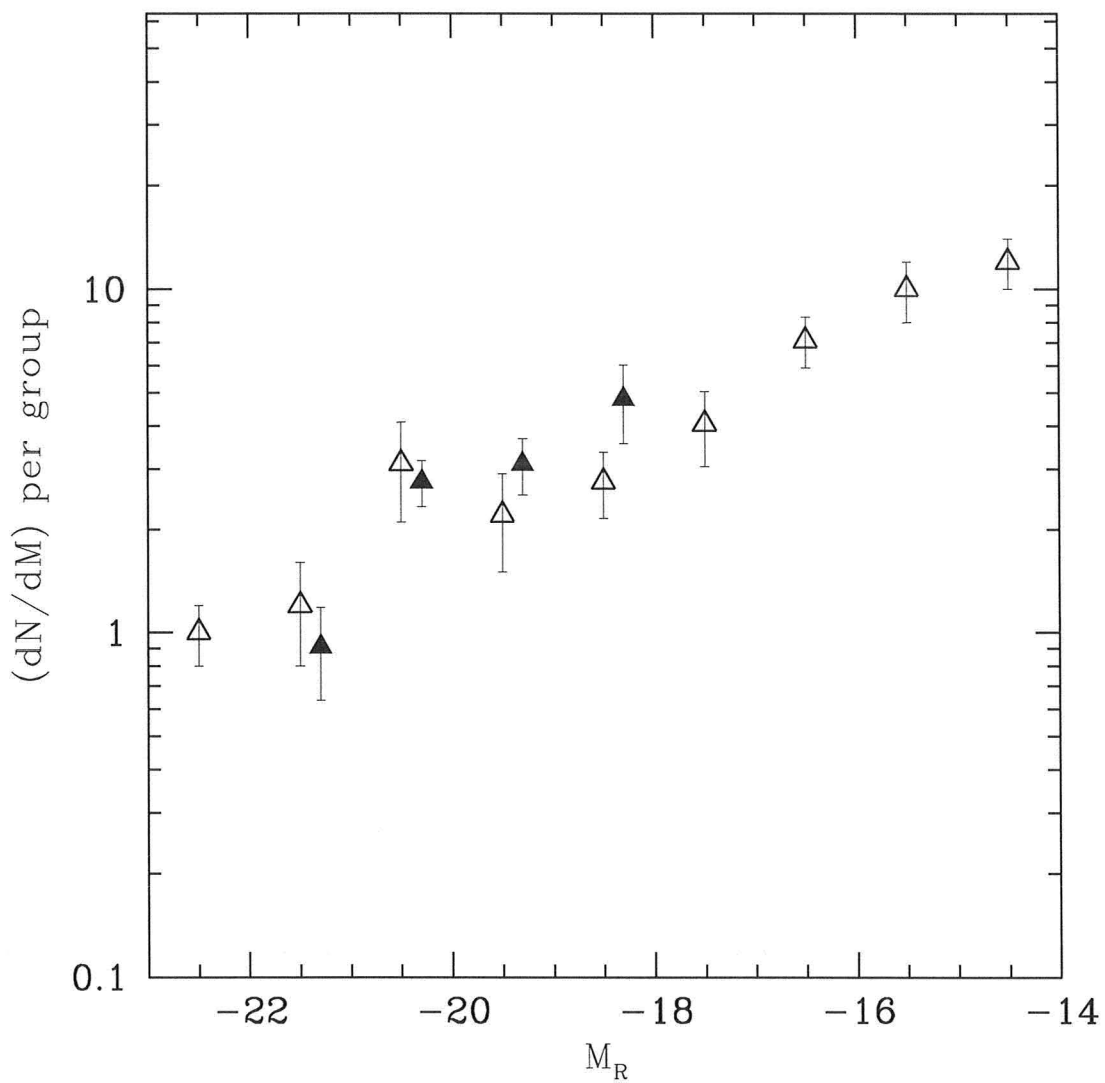


Figure 4.3: Analogous to Fig. 4.2. High- σ (or L_X) group LFs from the GEMS sample (empty triangles) and this work (filled triangles).

We can also examine how our red fraction-magnitude trend compares with a low- z sample, such as that from the SDSS groups (Weinmann et al., 2006), in which the group-finding algorithm is based on Yang et al. (2005). In their analysis of colour fractions, Weinmann et al. (2006) also found a trend of decreasing red fractions at fainter r -magnitudes. However, their group red fraction at the brighter magnitudes converged with a sample drawn from the full SDSS dataset (which includes field, group and cluster galaxies). This is in contrast with the current work, where we see convergence in the group and ‘field’ samples at fainter magnitudes. While our field sample is composed of all galaxies not in our groups, this may consist of galaxies in other groups, and is not a sample of purely isolated galaxies. We also do not have any large clusters in our fields.

4.3.2.1 Remarks on Faint Galaxies

In a study on red sequence galaxies in four clusters in the redshift range of $0.7 < z < 0.8$, De Lucia et al. (2004) found that there were remarkably few faint red galaxies populating their colour-magnitude diagrams. They surmise that star formation in the present-day red galaxies must have been truncated at times after $z = 0.8$, and in fact the blue galaxies in high- z clusters are likely candidates for their progenitors (Kodama & Bower, 2001). It also appears that faint red galaxies appear predominantly in clusters, rather than the field (Gilbank & Balogh, 2008). With faint red galaxies continuing to build up the red sequence at lower redshift, they provide excellent clues in characterising the star formation history of the Universe.

Chapter 5

Conclusions

In this thesis, we have presented an analysis of galaxy groups at intermediate redshift with the goal of characterising the faintest members. These faint galaxies were selected from the GEEC survey and targetted with the FORS2 instrument on the VLT to obtain redshift measurements in order to assign group members. From our sample of 10 GEEC groups, probing down to an apparent magnitude of $r = 23.25$, our main conclusions are:

- Group galaxies have consistently redder colours than the field.
- The faintest galaxies in our group and field environment have similar colours (primarily blue). This is a new result.
- Our luminosity functions indicate that the groups have more bright members, and possibly fewer faint members, than the field.
- There is no evidence to suggest that the overall shape of our luminosity functions are substantially different than similar group samples at low- z .
- Group galaxies appear to follow a trend of increasing red fraction with decreasing z , confirming previous work.

While additional data are necessary to make robust constraints on our results, our sample of faint galaxy group members provide compelling motivation that the faintest galaxies harbour key science. For example, both the group and field galaxies' red fractions begin to merge at the limits of our sample, and additional data will help to further characterise this observation.

5.1 Future Work

Our collaboration has access to a large set of data on galaxy groups at intermediate redshift, covering many filters. Only recently, we have obtained extensive observations with the GALEX telescope and will use these UV data to compute star formation rates for most of our galaxies. In addition, this will lead to robust calculations of stellar mass with the use of fitting procedures to characterise their spectral energy distributions (McGee, S. et al., in preparation).

Using these data, it will be possible to examine the star formation and stellar mass content of these fainter group members, which may provide clues to their role in the processes driving the truncation of star formation, and how they are transformed into red sequence galaxies. This can be further characterised by the 'dwarf-to-giant' ratio (DGR), as defined in De Lucia et al. (2004) and further studied by Gilbank & Balogh (2008). It appears that the field and cluster environment have similar DGR values at $z \sim 0$, whereas at higher z they were more discrepant. Computing the DGR for our sample will be a subject of future work.

In addition to extensions of our current dataset, the GEEC is also in the process of preparing a sample of galaxy groups selected from the SDSS catalogue, with the aim of obtaining a low- z dataset selected with the same group-finding algorithm as the $z \sim 0.4$ groups described in this thesis. This will allow fairer comparisons that are not biased by group selection. Furthermore, with the SDSS data and wider high- z surveys, we will be able to include the cluster environment in our comparisons. Viewing the properties that we have explored here and in other GEEC papers in such an expanded context is essential in deducing just how galaxy groups fit into the Universal picture of galaxy evolution.

5.2 Concluding Remarks

One of the most interesting reasons to study the smallest galaxies is the remarkable effect of cosmic downsizing, where the majority of the star formation in our Universe appears to be occurring in ever lower mass galaxies. Somehow, as the Universe evolves, galaxies are losing the ability to efficiently form stars. As we have seen, this truncation of star formation is recorded in part by a build-up of the red sequence, in which a large fraction of galaxies above a certain mass (or luminosity) have reddened, while galaxies below that mass remain predominantly blue. This trend evolves also with redshift. Studies, such as this thesis, are needed in order to probe these faint, star-forming galaxies, and ultimately we hope to uncover the processes which set them apart from their high-mass counterparts. While probing faint galaxies at significant distances is challenging, the information we can learn from these galaxies justifies

the effort. This work is the first to specifically probe very faint group galaxies at intermediate redshift, and will hopefully encourage similar future works.

Bibliography

Abazajian, K. N., Adelman-McCarthy, J. K., Agüeros, M. A., Allam, S. S., Allende Prieto, C., An, D., Anderson, K. S. J., Anderson, S. F., Annis, J., Bahcall, N. A., & coauthors, . 2009, *ApJS*, 182, 543

Athanassoula, E., Makino, J., & Bosma, A. 1997, *MNRAS*, 286, 825

Balogh, M., Eke, V., Miller, C., Lewis, I., Bower, R., Couch, W., Nichol, R., Bland-Hawthorn, J., Baldry, I. K., Baugh, C., Bridges, T., Cannon, R., Cole, S., Colless, M., Collins, C., Cross, N., Dalton, G., de Propris, R., Driver, S. P., Efstathiou, G., Ellis, R. S., Frenk, C. S., Glazebrook, K., Gomez, P., Gray, A., Hawkins, E., Jackson, C., Lahav, O., Lumsden, S., Maddox, S., Madgwick, D., Norberg, P., Peacock, J. A., Percival, W., Peterson, B. A., Sutherland, W., & Taylor, K. 2004a, *MNRAS*, 348, 1355

Balogh, M. L., Baldry, I. K., Nichol, R. C., Miller, C., Bower, R. G., & Glazebrook, K. 2004b, *ApJL*, 615, L101

Balogh, M. L. & McGee, S. L. 2010, *MNRAS*, 402, L59

Balogh, M. L., McGee, S. L., Wilman, D., Bower, R. G., Hau, G., Morris, S. L., Mulchaey, J. S., Oemler, Jr., A., Parker, L., & Gwyn, S. 2009, *MNRAS*, 398, 754

- Balogh, M. L., Wilman, D., Henderson, R. D. E., Bower, R. G., Gilbank, D., Whitaker, R., Morris, S. L., Hau, G., Mulchaey, J. S., Oemler, A., & Carlberg, R. G. 2007, MNRAS, 374, 1169
- Bell, E. F. & de Jong, R. S. 2001, ApJ, 550, 212
- Benson, A. J., Bower, R. G., Frenk, C. S., Lacey, C. G., Baugh, C. M., & Cole, S. 2003, ApJ, 599, 38
- Bertin, E. & Arnouts, S. 1996, A&AS, 117, 393
- Blaizot, J., Szapudi, I., Colombi, S., Budavári, T., Bouchet, F. R., Devriendt, J. E. G., Guiderdoni, B., Pan, J., & Szalay, A. 2006, MNRAS, 369, 1009
- Blanton, M. R. & Moustakas, J. 2009, ARA&A, 47, 159
- Blanton, M. R. & Roweis, S. 2007, AJ, 133, 734
- Bower, R. G. & Balogh, M. L. 2004, in Clusters of Galaxies: Probes of Cosmological Structure and Galaxy Evolution, from the Carnegie Observatories Centennial Symposia. Published by Cambridge University Press, as part of the Carnegie Observatories Astrophysics Series. Edited by J.S. Mulchaey, A. Dressler, and A. Oemler, 2004, p. 326., 326
- Bower, R. G., Benson, A. J., Malbon, R., Helly, J. C., Frenk, C. S., Baugh, C. M., Cole, S., & Lacey, C. G. 2006, MNRAS, 370, 645
- Carlberg, R. G., Yee, H. K. C., Ellingson, E., Morris, S. L., Abraham, R., Gravel, P., Pritchett, C. J., Smecker-Hane, T., Hartwick, F. D. A., Hesser, J. E., Hutchings, J. B., & Oke, J. B. 1997, ApJL, 485, L13

Carlberg, R. G., Yee, H. K. C., Morris, S. L., Lin, H., Hall, P. B., Patton, D. R., Sawicki, M., & Shepherd, C. W. 2001, *ApJ*, 552, 427

Cole, S., Lacey, C. G., Baugh, C. M., & Frenk, C. S. 2000, *MNRAS*, 319, 168

Cowie, L. L., Songaila, A., Hu, E. M., & Cohen, J. G. 1996, *AJ*, 112, 839

De Lucia, G., Poggianti, B. M., Aragón-Salamanca, A., Clowe, D., Halliday, C., Jablonka, P., Milvang-Jensen, B., Pelló, R., Poirier, S., Rudnick, G., Saglia, R., Simard, L., & White, S. D. M. 2004, *ApJ*, 610, L77

Dressler, A. 1980, *ApJ*, 236, 351

Dressler, A., Oemler, A. J., Couch, W. J., Smail, I., Ellis, R. S., Barger, A., Butcher, H., Poggianti, B. M., & Sharples, R. M. 1997, *ApJ*, 490, 577

Driver, S. P., Liske, J., Cross, N. J. G., De Propris, R., & Allen, P. D. 2005, *MNRAS*, 360, 81

Ebeling, H., Edge, A. C., & Henry, J. P. 2001, *ApJ*, 553, 668

Eke, V. R., Frenk, C. S., Baugh, C. M., Cole, S., Norberg, P., Peacock, J. A., Baldry, I. K., Bland-Hawthorn, J., Bridges, T., Cannon, R., Colless, M., Collins, C., Couch, W., Dalton, G., de Propris, R., Driver, S. P., Efstathiou, G., Ellis, R. S., Glazebrook, K., Jackson, C. A., Lahav, O., Lewis, I., Lumsden, S., Maddox, S. J., Madgwick, D., Peterson, B. A., Sutherland, W., & Taylor, K. 2004a, *MNRAS*, 355, 769

Eke, V. R. et al. 2004b, *MNRAS*, 348, 866

Ellison, S. L., Patton, D. R., Simard, L., & McConnachie, A. W. 2008, *AJ*, 135, 1877

Ellison, S. L., Patton, D. R., Simard, L., McConnachie, A. W., Baldry, I. K., & Mendel, J. T. 2010, *astroph*

Ellison, S. L., Simard, L., Cowan, N. B., Baldry, I. K., Patton, D. R., & McConnachie, A. W. 2009, *MNRAS*, 396, 1257

Felten, J. E. 1977, *AJ*, 82, 861

Finoguenov, A., Connelly, J. L., Parker, L. C., Wilman, D. J., Mulchaey, J. S., Saglia, R. P., Balogh, M. L., Bower, R. G., & McGee, S. L. 2009, *ApJ*, 704, 564

Fukugita, M., Shimasaku, K., & Ichikawa, T. 1995, *PASP*, 107, 945

Gómez, P. L., Nichol, R. C., Miller, C. J., Balogh, M. L., Goto, T., Zabludoff, A. I., Romer, A. K., Bernardi, M., Sheth, R., Hopkins, A. M., Castander, F. J., Connolly, A. J., Schneider, D. P., Brinkmann, J., Lamb, D. Q., SubbaRao, M., & York, D. G. 2003, *ApJ*, 584, 210

Gehrels, N. 1986, *ApJ*, 303, 336

Gerke, B. F., Newman, J. A., Faber, S. M., Cooper, M. C., Croton, D. J., Davis, M., Willmer, C. N. A., Yan, R., Coil, A. L., Guhathakurta, P., Koo, D. C., & Weiner, B. J. 2007, *MNRAS*, 376, 1425

Gilbank, D. G. & Balogh, M. L. 2008, *MNRAS*, 385, L116

Gladders, M. D. & Yee, H. K. C. 2000, *AJ*, 120, 2148

- Gorgas, J., Cardiel, N., Pedraz, S., & González, J. J. 1999, *A&AS*, 139, 29
- Hansen, S. M., Sheldon, E. S., Wechsler, R. H., & Koester, B. P. 2009, *ApJ*, 699, 1333
- Heavens, A., Panter, B., Jimenez, R., & Dunlop, J. 2004, *Nature*, 428, 625
- Hoekstra, H., Franx, M., Kuijken, K., Carlberg, R. G., Yee, H. K. C., Lin, H., Morris, S. L., Hall, P. B., Patton, D. R., Sawicki, M., & Wirth, G. D. 2001, *ApJL*, 548, L5
- Hopkins, A. M., Connolly, A. J., Haarsma, D. B., & Cram, L. E. 2001, *AJ*, 122, 288
- Hou, A., Parker, L. C., Harris, W. E., & Wilman, D. J. 2009, *ApJ*, 702, 1199
- Hubble, E. P. 1926, *ApJ*, 64, 321
- Huchra, J. P. & Geller, M. J. 1982, *ApJ*, 257, 423
- Jarrett, T. H., Chester, T., Cutri, R., Schneider, S., Skrutskie, M., & Huchra, J. P. 2000, *AJ*, 119, 2498
- Juneau, S., Glazebrook, K., Crampton, D., McCarthy, P. J., Savaglio, S., Abraham, R., Carlberg, R. G., Chen, H.-W., Le Borgne, D., Marzke, R. O., Roth, K., Jørgensen, I., Hook, I., & Murowinski, R. 2005, *ApJ*, 619, L135
- Kodama, T. & Bower, R. G. 2001, *MNRAS*, 321, 18
- Krajnović, D., Bacon, R., Cappellari, M., Davies, R. L., de Zeeuw, P. T., Em-
sellem, E., Falcón-Barroso, J., Kuntschner, H., McDermid, R. M., Peletier,

- R. F., Sarzi, M., van den Bosch, R. C. E., & van de Ven, G. 2008, MNRAS, 390, 93
- Lin, Y., Mohr, J. J., & Stanford, S. A. 2004, ApJ, 610, 745
- Lin, Y.-T., Mohr, J. J., & A., S. S. 2003, ApJ, 591, 749
- McConnachie, A. W., Ellison, S. L., & Patton, D. R. 2008, MNRAS, 387, 1281
- McGee, S. L., Balogh, M. L., Bower, R. G., Font, A. S., & McCarthy, I. G. 2009, MNRAS, 400, 937
- McGee, S. L., Balogh, M. L., Henderson, R. D. E., Wilman, D. J., Bower, R. G., Mulchaey, J. S., & Oemler, Jr., A. 2008, MNRAS, 387, 1605
- Miles, T. A., Raychaudhury, S., Forbes, D. A., Goudfrooij, P., Ponman, T. J., & Kozhurina-Platais, V. 2004, MNRAS, 355, 785
- Moss, C. & Whittle, M. 1993, ApJL, 407, L17
- Oke, J. B. & Sandage, A. 1968, ApJ, 154, 21
- Osmond, J. P. F. & Ponman, T. J. 2004, MNRAS, 350, 1511
- Parker, L. C., Hudson, M. J., Carlberg, R. G., & Hoekstra, H. 2005, ApJ, 634, 806
- Patton, D. R., Pritchet, C. J., Carlberg, R. G., et al. 2002, ApJ, 565, 208
- Peletier, R. & Balcells, M. 1996, in *Spiral Galaxies in the Near-IR*, Proceedings of the ESO/MPA Workshop Held at Garching, Germany, 7-9 June 1995

edited by Dante Minniti and Hans-Walter Rix. Springer-Verlag Berlin Heidelberg New York. Also ESO Astrophysics Symposia (European Southern Observatory), 1996., p.48, ed. D. Minniti & H.-W. Rix, 48–+

Postman, M. & Geller, M. J. 1984, *ApJ*, 281, 95

Proctor, R. N., Sansom, A. E., & Reid, I. N. 2000, *MNRAS*, 311, 37

Quilis, V., Moore, B., & Bower, R. 2000, *Science*, 288, 1617

Ramella, M., Boschin, W., Geller, M. J., Mahdavi, A., & Rines, K. 2004, *AJ*, 128, 2022

Ramella, M., Zamorani, G., Zucca, E., Stirpe, G. M., Vettolani, G., Balkowski, C., Blanchard, A., Cappi, A., Cayatte, V., Chincarini, G., Collins, C., Guzzo, L., MacGillivray, H., Maccagni, D., Maurogordato, S., Merighi, R., Mignoli, M., Pisani, A., Proust, D., & Scaramella, R. 1999, *A&A*, 342, 1

Rees, M. J. & Ostriker, J. P. 1977, *MNRAS*, 179, 541

Rieke, G. H., Young, E. T., Engelbracht, C. W., Kelly, D. M., Low, F. J., Haller, E. E., Beeman, J. W., Gordon, K. D., Stansberry, J. A., Misselt, K. A., Cadien, J., Morrison, J. E., Rivlis, G., Latter, W. B., Noriega-Crespo, A., Padgett, D. L., Stapelfeldt, K. R., Hines, D. C., Egami, E., Muzerolle, J., Alonso-Herrero, A., Blaylock, M., Dole, H., Hinz, J. L., Le Floc'h, E., Papovich, C., Pérez-González, P. G., Smith, P. S., Su, K. Y. L., Bennett, L., Frayer, D. T., Henderson, D., Lu, N., Masci, F., Pesenson, M., Rebull, L., Rho, J., Keene, J., Stolovy, S., Wachter, S., Wheaton, W., Werner, M. W., & Richards, P. L. 2004, *ApJS*, 154, 25

Robaina, A. R., Bell, E. F., Skelton, R. E., McIntosh, D. H., Somerville, R. S., Zheng, X., Rix, H., Bacon, D., Balogh, M., Barazza, F. D., Barden, M., Böhm, A., Caldwell, J. A. R., Gallazzi, A., Gray, M. E., Häussler, B., Heymans, C., Jahnke, K., Jogee, S., van Kampen, E., Lane, K., Meisenheimer, K., Papovich, C., Peng, C. Y., Sánchez, S. F., Skibba, R., Taylor, A., Wisotzki, L., & Wolf, C. 2009, *ApJ*, 704, 324

Schechter, P. 1976, *ApJ*, 203, 297

Schlegel, D. J., Finkbeiner, D. P., & Davis, M. 1998, *ApJ*, 500, 525

Simard, L., Willmer, C. N. A., Vogt, N. P., Sarajedini, V. L., Phillips, A. C., Weiner, B. J., Koo, D. C., Im, M., Illingworth, G. D., & Faber, S. M. 2002, *ApJS*, 142, 1

Sparke, L. S. & Gallagher, III, J. S. 2007, *Galaxies in the Universe: An Introduction*, ed. Sparke, L. S. & Gallagher, J. S., III (Cambridge University Press)

Strateva, I., Ivezić, Ž., Knapp, G. R., Narayanan, V. K., Strauss, M. A., Gunn, J. E., Lupton, R. H., Schlegel, D., Bahcall, N. A., Brinkmann, J., Brunner, R. J., Budavári, T., Csabai, I., Castander, F. J., Doi, M., Fukugita, M., Györy, Z., Hamabe, M., Hennessy, G., Ichikawa, T., Kunszt, P. Z., Lamb, D. Q., McKay, T. A., Okamura, S., Racusin, J., Sekiguchi, M., Schneider, D. P., Shimasaku, K., & York, D. 2001, *AJ*, 122, 1861

Terndrup, D. M. 1993, in *ASP Conf. Ser. 39: The Minnesota Lectures on the Structure and Dynamics of the Milky Way*, ed. R. M. Humphreys, 9–+

- Visvanathan, N. & Sandage, A. 1977, *ApJ*, 216, 214
- Weinmann, S. M., van den Bosch, F. C., Yang, X., Mo, H. J., Croton, D. J., & Moore, B. 2006, *MNRAS*, 372, 1161
- White, S. D. M. & Frenk, C. S. 1991, *ApJ*, 379, 52
- White, S. D. M. & Rees, M. J. 1978, *MNRAS*, 183, 341
- Wilman, D. J., Balogh, M. L., Bower, R. G., Mulchaey, J. S., Oemler, A., Carlberg, R. G., Eke, V. R., Lewis, I., Morris, S. L., & Whitaker, R. J. 2005a, *MNRAS*, 358, 88
- Wilman, D. J., Balogh, M. L., Bower, R. G., Mulchaey, J. S., Oemler, A., Carlberg, R. G., Morris, S. L., & Whitaker, R. J. 2005b, *MNRAS*, 358, 71
- Wilman, D. J., Oemler, A., Mulchaey, J. S., McGee, S. L., Balogh, M. L., & Bower, R. G. 2009, *ApJ*, 692, 298
- Yang, X., Mo, H. J., van den Bosch, F. C., & Jing, Y. P. 2005, *MNRAS*, 356, 1293
- Yee, H. K. C., Morris, S. L., Lin, H., Carlberg, R. G., Hall, P. B., Sawicki, M., Patton, D. R., Wirth, G. D., Ellingson, E., & Shepherd, C. W. 2000, *ApJS*, 129, 475
- York, D. G., Adelman, J., Anderson, Jr., J. E., Anderson, S. F., Annis, J., Bahcall, N. A., Bakken, J. A., Barkhouser, R., Bastian, S., Berman, E., & coauthors, . 2000, *AJ*, 120, 1579

